The Unusual Early Morning Tornado in Ciudad Acuña, Coahuila, Mexico, on 25 May 2015

BRADFORD S. BARRETT

Oceanography Department, U.S. Naval Academy, Annapolis, Maryland, and Centro de Ciencias de la Atmósfera, Universidad Nacional Autónoma de México, Ciudad de México, Mexico

LUIS M. FARFÁN

Unidad La Paz, Centro de Investigación Científica y de Educación Superior de Ensenada, Ensenada, Baja California, Mexico

GRACIELA B. RAGA AND DARIBEL H. HERNÁNDEZ

Centro de Ciencias de la Atmósfera, Universidad Nacional Autónoma de México, Ciudad de México, Mexico

(Manuscript received 1 July 2016, in final form 8 December 2016)

ABSTRACT

This study analyzes the synoptic- and mesoscale conditions present during initiation and intensification of the supercell thunderstorm that produced a tornado in Ciudad Acuña, a community located in the state of Coahuila, Mexico, 10 km southwest of the U.S. border. Early morning convective activity, first detected by radar at 0628 UTC 25 May 2015, developed into an intense and well-defined supercell thunderstorm that produced a tornado between approximately 1045 and 1130 UTC. Hourly analyses from the Rapid Refresh model indicated an upslope component to surface flow in the region of convection initiation over the Serranías del Burro (SdB). Along the storm's trajectory, dewpoint temperatures increased from 15° to 22°C, convective available potential energy increased from 1500 to near 4000 J kg^{-1}, and convective inhibition changed from −150 J kg^{-1} at the time of convection initiation to near zero in Ciudad Acuña. Simulations from the Weather Research and Forecasting Model confirmed the sensitivity of both convection initiation and storm intensification to the topography of the SdB. In the control simulation and two simulations in which topography was reduced in elevation, a cluster of storms formed and intensified over the central mountains. However, when topography was further reduced and the SdB region became a large flat plain, little convective activity was seen, forming only along the dryline without intensifying or propagating to the east as was observed.

1. Introduction

During the overnight hours of 25 May 2015, a thunderstorm initiated over the Serranías del Burro (SdB) region of northern Coahuila State, in northern Mexico. That thunderstorm went on to become supercellular and eventually tornadic, with tornado damage and fatalities reported in the city of Ciudad Acuña 10 km southwest of the Mexico–U.S. border in the hour before sunrise. Two unusual aspects of that severe weather event motivated this study. First, as will be shown later, the thunderstorm formed, intensified, and became tornadic all during the overnight hours, a fairly atypical evolution for tornadic thunderstorms (Ashley et al. 2008; Kis and Straka 2010). Second, the thunderstorm formed in the SdB, an area identified as favorable for daytime convection by Edwards (2006, hereafter E06) and Weiss and Zeitler (2008, hereafter WZ08) but not examined in depth for nocturnal convection. As discussed in greater detail below, the environment on 25 May 2015 exhibited some of the characteristics identified by Mead and Thompson (2011) (e.g., a strong low-level jet and moderate convective instability) and Kis and Straka (2010) (e.g., substantial low-level shear and storm-relative helicity) as favorable for nocturnal tornadoes. The environment was also found to have surface winds with an upslope flow component, and surface upslope flow was identified by Barthlott et al. (2006) as one possible triggering mechanism for convective cells. The primary goal of this

Corresponding author: Dr. Graciela B. Raga, raga.graciela@gmail.com

DOI: 10.1175/MWR-D-16-0252.1

study was to explore these environmental conditions and physical mechanisms associated with the initiation and intensification of this nocturnal tornadic supercell.

Nocturnal tornadoes remain relatively understudied, despite comprising about 25% of all tornadoes and accounting for over 40% of tornado casualties (Ashley 2007). Indeed, few climatological studies of tornadoes have discriminated between daytime and nocturnal events, exceptions being Skaggs (1969), Maddox (1983), Davies and Fischer (2009), and Kis and Straka (2010). Many of the ''recipe based'' approaches used to discriminate environmental conditions (sometimes called ''ingredients'') favorable to tornado occurrence have tended either to focus on tornadoes in the afternoon and evening or else to not differentiate tornado environments by time of day (Fawbush and Miller 1952; Maddox 1976; Davies and Johns 1993; Brooks et al. 1994; Rasmussen and Blanchard 1998; Rasmussen 2003; Thompson et al. 2003; Potvin et al. 2010). One such ingredient, low-level shear, has been observed to reach a climatological maximum in the early morning hours in the U.S. southern and central plains, largely as a result of nocturnal stratification of the boundary layer (Bonner 1968; Zhong et al. 1996; Whiteman et al. 1997; Parish and Oolman 2010). However, nocturnal tornadic events tend not to be characterized by large stable stratification in the boundary layer (Mead and Thompson 2011). Instead, the increased low-level shear tends to be the result of exceptionally strong low-level jets (Kis and Straka 2010). Lower troposphere height falls associated with the approach of a midtropospheric vorticity maximum (such as was the case on 25 May 2015) are one mechanism for low-level jet formation (Chen and Kpaeyeh 1993). Furthermore, a region characterized by gently sloping terrain (such as the eastern slopes of the SdB) also favors the formation of a nocturnal low-level jet (McNider and Pielke 1981; Shapiro and Fedorovich 2009; Shapiro et al. 2016). A thunderstorm that can initiate in a favorable thermodynamic environment with a strong low-level jet, and thus strong low-level shear, can become supercellular and tornadic. Upslope flow is one possible mechanism that can aid in convection initiation (Smith 1979; Houze 1993; Lin 1993; Chu and Lin 2000; Bluestein 2000), and the geography of the SdB region ensures that lower-troposphere winds from the southeast will have an upslope component.

Upslope flow was mentioned by E06 and WZ08 as a possible mechanism for convection initiation in the SdB, but it was not explored significantly in either climatological study. The E06 climatology used observations from the Laughlin Air Force Base (KDFX) WSR-88D to document 13 supercell thunderstorms between February 2004 and May 2006. All but two of those supercell events occurred from February to May; the other two events occurred in October and November. All 13 events in the E06 climatology occurred in the late afternoon and early evening, ranging from 2000 to 0400 UTC (1500–2300 LT). E06 did note that a potentially tornadic signature in KDFX base reflectivity was observed at 0540 UTC (0040 LT) 22 March 2000, although that was the only nighttime supercell event mentioned by E06, and it was not included in the climatology. All 13 supercell cases analyzed by E06 were characterized by very similar synoptic-scale environments: broadly southwesterly mid- and upper-tropospheric flow located over northern Coahuila State and a trough located within 1000 km to the west of the state. The mean storm motion at mature phase for the 13 events was from west to east, and the mean storm speed was 17.4 kt ($1\,\text{kt} = 0.5144\,\text{m s}^{-1}$). A composite sounding of the events, based on vertical profiles from either the Del Rio, Texas (KDRT), observational sounding or the nearest grid point of the Rapid Update Cycle (RUC) numerical weather prediction model, showed mean surface-based convective available potential energy (CAPE) of $2709\,\text{J kg}^{-1}$, mean surface-based convective inhibition (CIN) of $-70\,\text{J kg}^{-1}$, a surface to 6-km bulk wind difference (BWD) of 49 kt, surface to 1-km storm-relative helicity (SRH) of $116\,\text{m}^2\,\text{s}^{-2}$, and surface to 3-km SRH of $157\,\text{m}^2\,\text{s}^{-2}$. These instability and shear values compare favorably to the climatological studies of Rasmussen and Blanchard (1998), Thompson et al. (2003), Rasmussen (2003), and Potvin et al. (2010), indicating afternoon and evening Coahuila supercell events resemble afternoon and evening severe events from other parts of the United States.

In a broader study, WZ08 documented 76 supercell thunderstorms from January 1996 to May 2007 in the SdB region, an average of about 8 supercells per year. The median onset time of the supercells in WZ08 was 2308 UTC (1808 LT), and 92% of the supercells selected for their study had formed by 0500 UTC (0000 LT). WZ08 found that the median lifetime for supercells that formed over the SdB was 94 min, about the same duration as the average found by Burgess et al. (1982) for all supercells in the United States. No early morning events were included in the WZ08 climatology, despite anecdotal evidence from E06 of at least one nocturnal event in the region. The WZ08 climatology suggests strong surface heating as being one of the most important contributors to deep convection formation over the SdB region. However, for the 25 May 2015 case, solar insolation and an elevated heat source were absent, meaning another forcing mechanism, including on either the synoptic scale or mesoscale or both, was responsible for the initiation of

thunderstorms around 0630 UTC (0130 LT). Those synoptic and mesoscale conditions present prior to and during the tornado event are analyzed in this study. Furthermore, sensitivity of convection initiation, development, and propagation to topography is tested in numerical simulations, with the goal to better understand the nocturnal tornado event. The remainder of this article is organized as follows: a description of datasets and model setup used to analyze the event are presented in section 2. In section 3, the evolution of the thunderstorm and supercell as seen in radar observations is discussed. In section 4, the synoptic and mesoscale environment of the supercell event are described from an observational perspective. Results from numerical simulations are presented in section 5. Finally, conclusions are presented in section 6.

2. Data and model description

To understand the synoptic- and mesoscale environment of this tornado event, fields of geopotential height and wind at 500 and 850 hPa, along with 2-m dewpoint temperature and 10-m wind $\mathbf{u}_{10m}$, were examined at 0000 and hourly from 0600 to 1200 UTC 25 May 2015 (1900 LT 24 May 2015 and hourly from 0100 to 0700 LT 25 May 2015) from the Rapid Refresh (RAP; Benjamin et al. 2006) model analyses with 13-km horizontal resolution. The upslope surface flow component was calculated as the scalar product between the 10-m wind vector $\mathbf{u}_{10m}$ and the horizontal gradient of terrain elevation z: $\mathbf{u}_{10m} \cdot \nabla z$. Positive values indicated upslope flow and negative values indicated downslope flow. Horizontal surface mass convergence was calculated as $-\nabla \cdot \rho \mathbf{u}_{10m}$, where ρ represents moist air density at 2 m, following Banacos and Schultz (2005). Positive values indicated horizontal convergence and negative values indicated divergence. Hourly environmental conditions immediately upstream of the storm were calculated by averaging values of the nine RAP grid points centered 25 km to the southeast of the storm position at that hour.

The base reflectivity, base velocity, and correlation coefficient at the 0.5° elevation angle of the KDFX WSR-88D were examined from 0600 to 1200 UTC. Radial wind differences were calculated at each radar time step as differences between the largest positive and largest negative base velocities in a 25 km × 25 km region approximately centered on the base reflectivity hook echo. This methodology is similar to the low-level delta velocity calculation of Kingfield and LaDue (2015) and the rotational velocity calculation of Smith et al. (2015), although here the maximum values were constrained only to be near the hook echo region, not lie on adjacent radials (Kingfield and LaDue 2015) or radials within 5 nm of each other (Smith et al. 2015). Because the radial wind differences were calculated manually, the authors were able to ensure that none was primarily convergent or divergent. All of the largest positive and largest negative radial velocities were located within 10 km of each other, and it should be noted that the 0.5° elevation angle imparted a slight vertical slope to the radial wind observations.

The 0000 and 1200 UTC 25 May 2015 KDRT soundings from the upper-air observing station at Del Rio were also examined. The 1200 UTC 25 May 2015 sounding served as an excellent (e.g., Potvin et al. 2010) proximity sounding, sampling the thermodynamical and dynamical environments only 50 km upstream of the supercell thunderstorm.

And finally, strong in-cloud and cloud-to-ground lightning flashes detected by the World Wide Lightning Location Network (WWLLN; Lay et al. 2004) were used as a measure of supercell intensification. A summary of the observing stations, topographic features, and political boundaries of the region is presented in Fig. 1.

Simulations of the event were performed using the Weather Research and Forecasting (WRF) Model (Skamarock et al. 2008), version 3.7.1, to better understand the potential for upslope flow to serve as the forcing mechanism for convection initiation. WRF is a three-dimensional nonhydrostatic regional numerical weather prediction model, and the simulations are performed using one coarse grid and two nested domains. The horizontal grid spacing for the three domains was 9, 3, and 1 km, respectively, with 45 irregularly spaced vertical sigma levels and a 50-hPa model top. Simulations were initialized at 0000 UTC 24 May 2015 and were run for 48 h. Initial and boundary conditions were provided by the North American Mesoscale Forecast System (NAM) at 12-km horizontal resolution as well as 3-hourly updates with respect to the initialization time (0000 UTC 24 May). No updates were taken from subsequent forecast cycles. The following physical parameterizations were used: the microphysics scheme by Lin et al. (1983), the four-layer Noah land surface model (Chen and Dudhia 2001), the Dudhia (1989) parameterization for shortwave radiation, the Rapid Radiative Transfer Model (Mlawer et al. 1997) for longwave radiation, and the Yonsei University (Hong et al. 2006) parameterization for the planetary boundary layer. Additionally, the Grell–Devenyi (Grell and Devenyi 2002) cumulus parameterization was used for the coarser domain (9 km) and no cumulus parameterization was applied to the two nested grids.

Four simulations of the event were performed. A control simulation used all of the settings as described above. The other three simulations adjusted the model

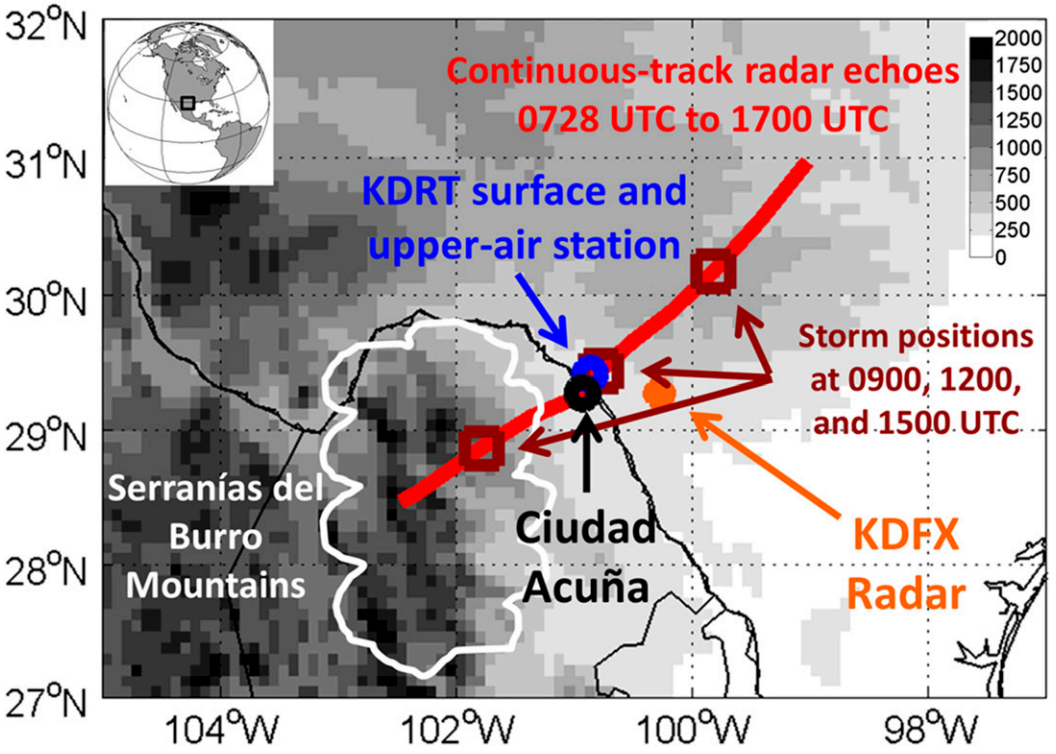

FIG. 1. Orientation schematic for stations and geographic features of the region of study. Shading is topography (m MSL; terrain elevations given in legend in upper right). The SdB are indicated by white scalloping. Orange dot gives the location of KDFX WSR-88D, and blue dot gives the location of KDRT upper-air and surface station. Red line indicates track of continuous base reflectivity echoes at 0.5° tilt between 0728 and 1700 UTC 25 May 2015. Dark red circles are storm positions at 0900, 1200, and 1500 UTC, and black circle notes the position of Ciudad Acuña.

topography of the SdB region (bounded by 28°–30°N, 101°–103°W) successively lower than in the control simulation: first to 75% of the original height, then to 50%, then finally to 25% (Fig. 2). This method is similar to the method of Barrett et al. (2009), but in this study, all elevations in the SdB region above a threshold were set to that threshold value. The thresholds were as follows: 1878 m for the 75% experiment (that height was selected because 1878 m is 75% of the maximum height in the bounded region in the control simulation), 1252 m in the 50% experiment, and 626 m in the 25% simulation. These adjustments effectively created smaller mountains in the 75% experiment, a tall mesa in the 50% experiment, and in the 25% experiment the entire SdB region resembled one continuous flat plain that gently sloped downward to the east (Fig. 2). Once the terrain elevations in the bounded region in the 1-km domain were flattened to their respective percentages, the edges of the bounded region were smoothed using a cubic kernel smoother to remove any abrupt height changes associated with the modification of the terrain. Then, the 1-km domain terrain was upscaled onto the 3-km domain grid using bilinear interpolation. In the 3-km domain, the 10 grid points on either side of the edge of the data from the 1-km domain were then smoothed using a seven-point cubic kernel smoother, again to remove any abrupt height changes associated with terrain edits. Finally, terrain from the 3-km domain was then upscaled onto the outer 9-km domain grid using the same method to upscale the 1-km domain onto the 3-km one. Several different smoothing and interpolation techniques were tested. The seven-point kernel smoother was selected because it provided the least-abrupt transition between the domain edges.

3. Radar-based evolution of the Ciudad Acuña thunderstorm

Convection initiation, determined by the first base reflectivity echoes over 20 dBZ from the KDFX radar, occurred at 0628 UTC (at the 0.5° elevation angle), and at that hour the radar switched from clear-air to precipitation scanning mode (e.g., Fulton et al. 1998). At 0728 UTC (0228 LT; Fig. 3a), reflectivity values near 45 dBZ from those original storms were seen over the eastern slopes of the SdB. Furthermore, at that time, the

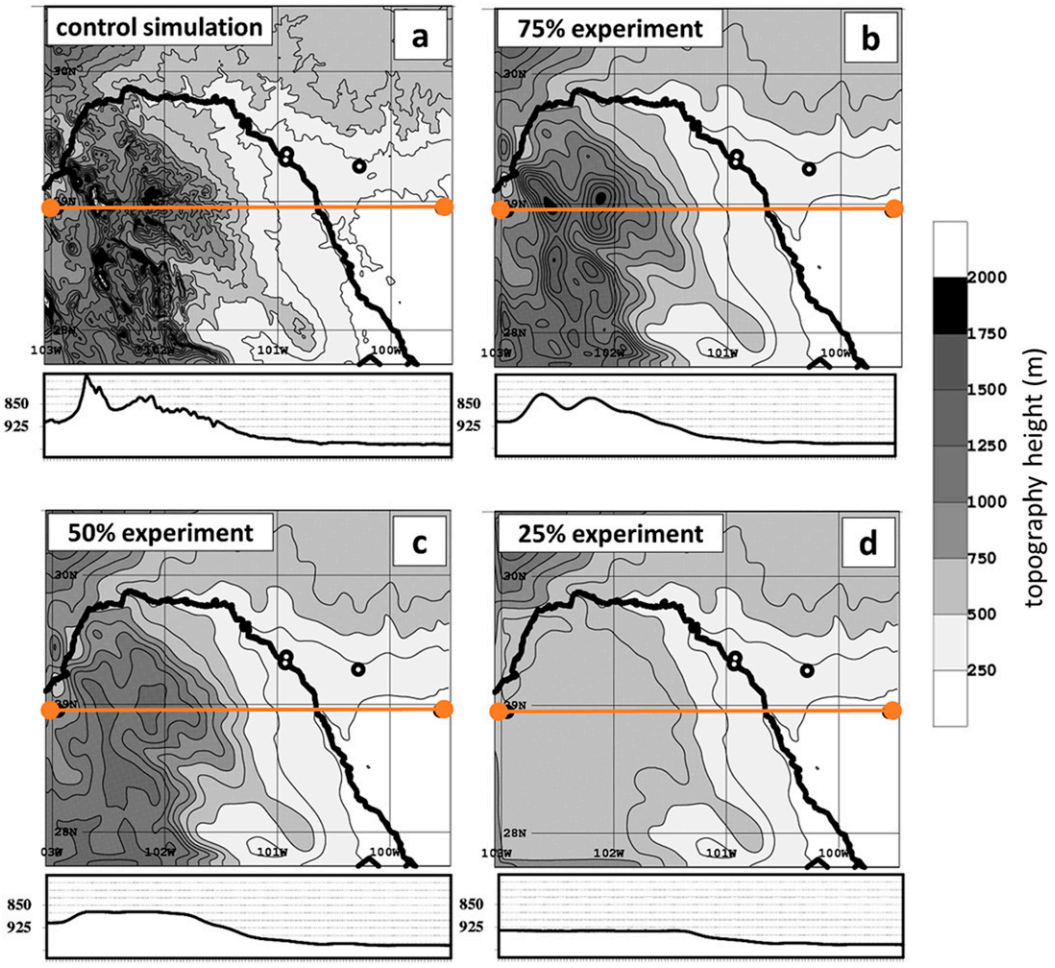

FIG. 2. Topography (shaded, m) for four sensitivity simulations performed using the WRF Model: (a) control with 100% elevations, (b) elevations reduced to 75%, (c) elevations reduced to 50%, and (d) elevations reduced to 25%. Vertical profiles (pressure, hPa) are below each panel, along 28.95°N and indicated by orange lines.

first reflectivity returns of the thunderstorm that eventually produced the Ciudad Acuña tornado were seen over the central SdB (indicated by a black arrow in Fig. 3a). This initial convective activity was mentioned in Mesoscale Discussion 0757 (available online at http://www.spc.noaa.gov/products/md/2015/md0757.html), issued at 0817 UTC by the U.S. Storm Prediction Center (SPC), which highlighted the potential for continued intensification of convection over northern Coahuila and potential morning tornado risk. Over the next 2 h from 0728 to 0930 UTC (Figs. 3b and 3c), disorganized convection that would later produce the supercell and tornado in Ciudad Acuña moved northeast and steadily increased in organization. By 0930 UTC, base reflectivity (0.5° elevation) exceeded 50 dBZ. Other cellular convection was noted to the east and north of this storm, including the original convective element detected at 0628 UTC, but this convective activity steadily decreased in reflectivity intensity between 0832 and 0930 UTC. Between 0930 and 1032 UTC (Figs. 3c and 3d), the storm underwent a significant transformation in base reflectivity, and its maximum dBZ reached 65. At 1022 UTC, the storm resembled a kidney bean shape in base reflectivity, and that shape has been associated with high-precipitation supercell thunderstorms (e.g., Przybylinski et al. 1993; Moller et al. 1994; McCaul et al. 2002; Thompson et al. 2003). This increase in convective organization seen in base reflectivity was associated with a significant increase in lightning flash activity. From 0700 to 1000 UTC, 93, 31, and 92 flashes were detected each hour, respectively, in a domain centered in northern Coahuila (Fig. 4). However, from 1000 to 1100 UTC, 2269 flashes were detected, an increase often associated with enhanced convective intensity (Steiger et al. 2007; Deierling and Peterson 2008). From 1032 to 1231 UTC (Figs. 3d–f and 4), the

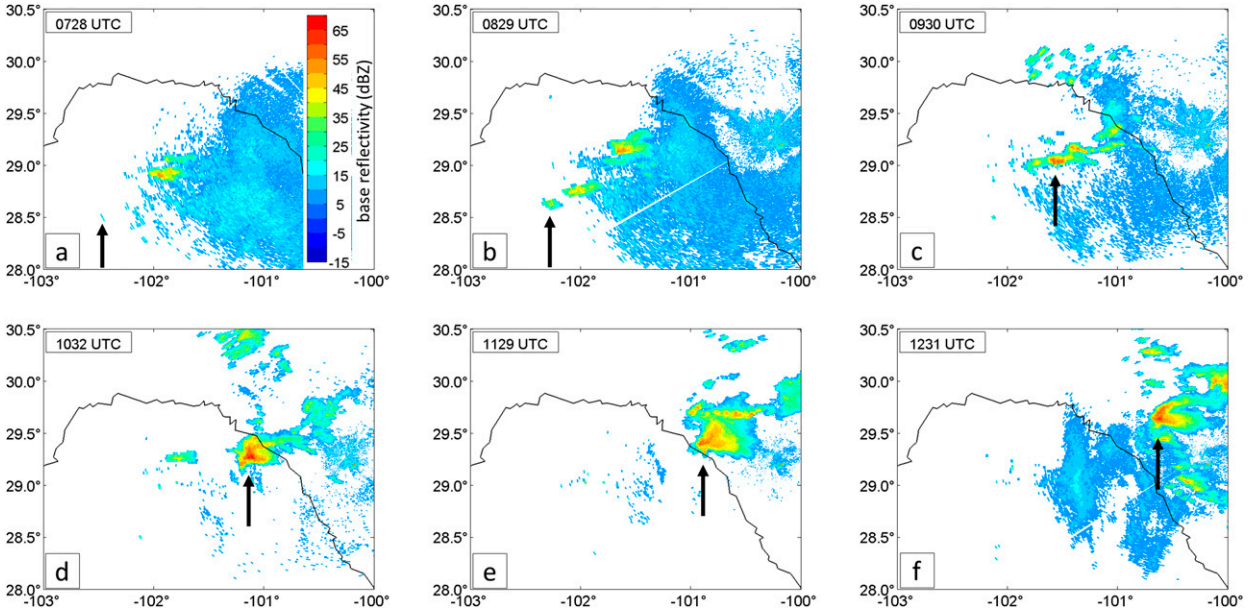

FIG. 3. Base reflectivity (dBZ) at 0.5° tilt from KDFX WSR-88D. All times in UTC (subtract 5 h from UTC for local hour) on 25 May 2015. Black arrows indicate the thunderstorm that produced the Ciudad Acuña tornado (tornado occurred between approximately 1045 and 1130 UTC).

supercell moved east-northeastward across Ciudad Acuña, Coahuila, and Del Rio.

From 1022 to 1032 UTC (Figs. 5a–f), the supercell began to exhibit a hooklike feature in base reflectivity on its southern and southwestern flank, a feature often associated with the presence of a mesocyclone (Fujita 1965; Forbes 1981; Markowski 2002). However, radial wind differences indicative of low-level rotation were small (or radial velocities missing) (Figs. 5b and 5e) in 0.5° elevation base velocity. Starting at 1042 UTC and continuing through 1124 UTC, the supercell exhibited both the hooklike feature in base reflectivity (Figs. 5g, 5j, 6a, 6d, and 6g) and radial wind differences associated with low-level rotation of a mesocyclone (Figs. 5k, 6b, 6e, and 6h). The radial wind difference in 0.5° elevation base velocity stayed at or above 45 m s^{-1} from 1042 to 1124 UTC and peaked at 85 m s^{-1} at 1113 UTC (Fig. 6e). This 85 m s^{-1} difference was the result of +50 m s^{-1} flow away from KDFX adjacent to −35 m s^{-1} flow toward KDFX. This very strong low-level radial wind difference was likely associated with the parent mesocyclone of the tornado, similar to Dunn and Vasiloff (2001, their Fig. 17f). The 42-min window (1042–1124 UTC) of strong low-level radial wind difference detected in radar corroborated local reports from the Civil Defense Agency of Coahuila that tornado damage began at approximately 1045 UTC and ended at approximately 1130 UTC. The occurrence of a tornado was supported by eyewitness video of a rope-stage tornado in the predawn light at approximately 1120 UTC (viewed by the authors, but not shown here). Additionally, damage surveys from the Mexican National Water Commission [Comisión Nacional del Agua (CONAGUA)] indicated the tornado may have

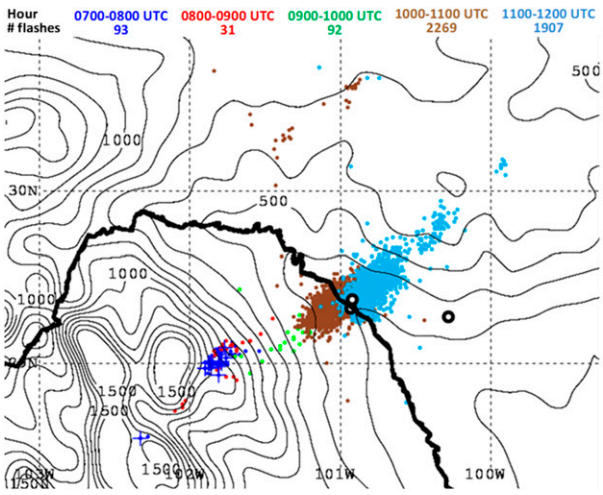

FIG. 4. In-cloud and cloud-to-ground lightning flashes detected per hour from 0700 to 1200 UTC 25 May 2015. Colors correspond to time of flash (UTC)—blue: 0700–0800, red: 0800–0900, green: 0900–1000, brown: 1000–1100, light blue: 1100–1200—and respective counts of flashes in the region shown reported in the table at the top of each panel. Positions of Ciudad Acuña, Del Rio upper-air station, and KDFX radar are indicated by circles. Topography height contoured every 100 m.

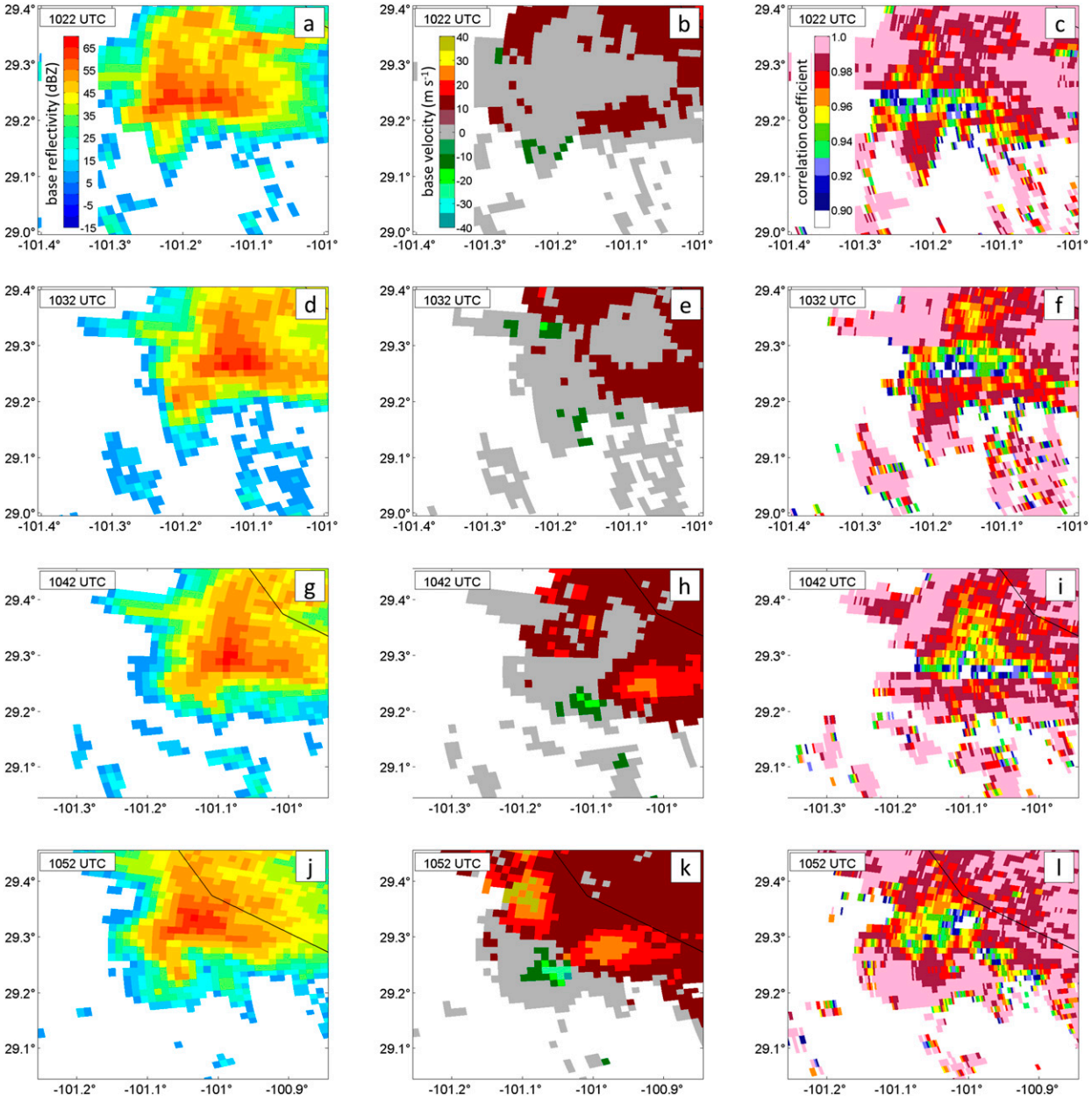

FIG. 5. (left) Base reflectivity (dBZ), (middle) base velocity (m s^{-1}), and (right) correlation coefficient at 0.5° elevation angle from KDFX WSR-88D at (a)–(c) 1022, (d)–(f) 1032, (g)–(i) 1042, and (j)–(l) 1052 UTC 25 May 2015, zoomed to the storm position at each time.

produced winds to 200 km h^{-1} (*Excelsior*, 6 April 2015), or between EF2 and EF3 on the enhanced Fujita (EF) scale, although it is important to recognize the difficulty of assigning wind speed ranges based on damage indicators (Doswell et al. 2009). Between 1124 and 1134 UTC (Figs. 6g–l), the supercell changed character, losing strong low-level rotation while moving out of Coahuila and into Texas. From 1200 to 1300 UTC 25 May 2015, the thunderstorm remained isolated (Fig. 3f), and maximum reflectivity remained above 55 dBZ. However, no tornadoes were reported in the United States along its track, although two severe hail reports were made in Texas, one (1.00-in. diameter) in Del Rio at 1119 UTC and another near Carta Valley in Edwards County (1.50-in. diameter) at 1315 UTC (reports taken from the National Centers for Environmental Information Storm Events Database, online at https://www.ncdc.noaa.gov/stormevents/). It is possible that the supercell thunderstorm produced no new tornadoes once in Texas because it moved into a

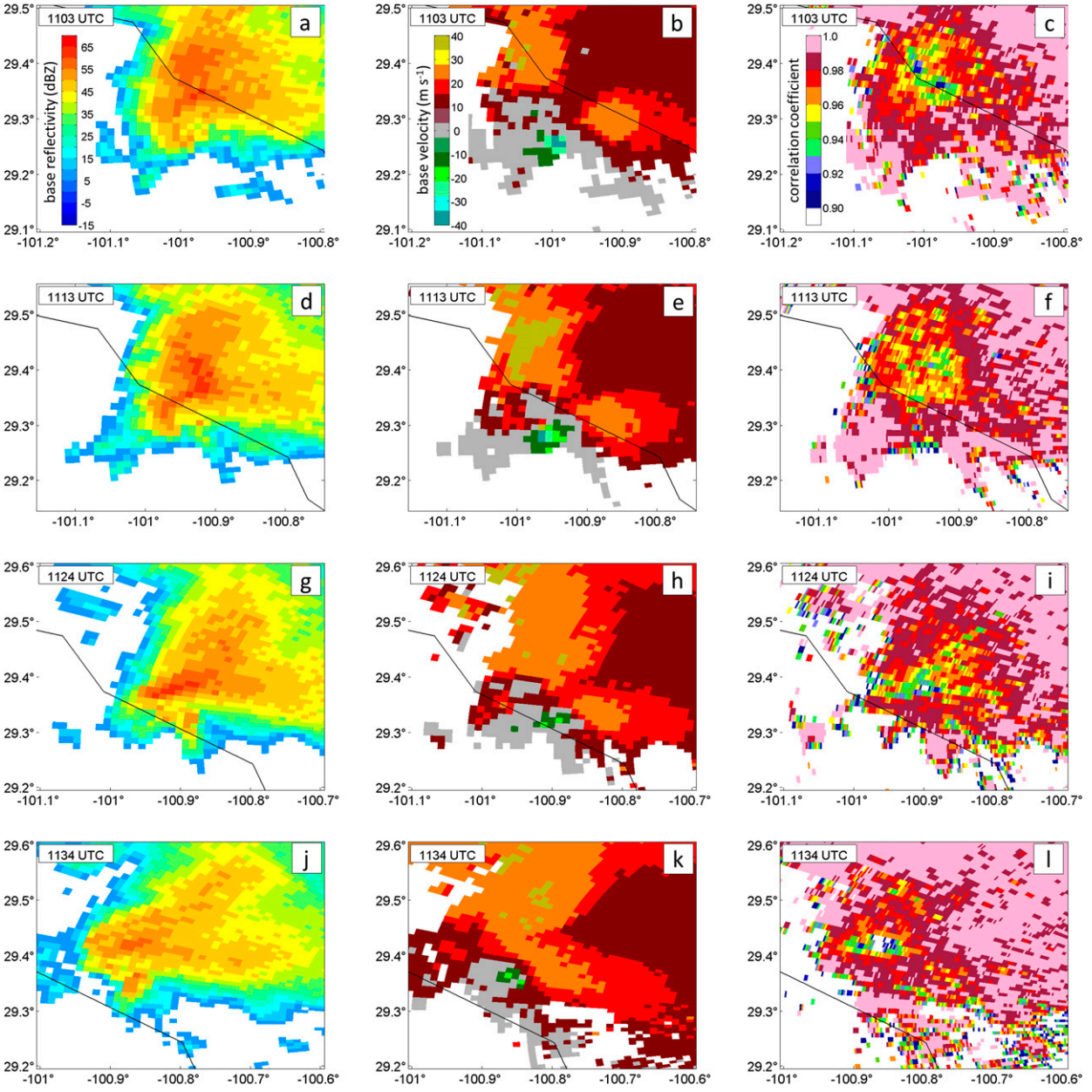

FIG. 6. As in Fig. 5, but for 1103, 1113, 1124, and 1134 UTC 25 May 2015.

region of higher CIN, as mentioned by the SPC in Mesoscale Discussion 0757.

4. Synoptic and mesoscale environment before, during, and after convection initiation

a. Preconvection environment

The evolution of synoptic-scale conditions from 0000 UTC 25 May 2015 through 1200 UTC 25 May 2015 (from approximately 7 h prior to the formation of the first thunderstorms over the SdB to approximately 30 min after the dissipation of the tornado in Ciudad Acuña) was as follows. At 0000 UTC, a closed low was analyzed at 500 hPa over south-central Wyoming within a long-wave trough extending across much of the Rocky Mountains region (Fig. 7a). Two short-wave troughs were also analyzed, one centered over northwestern Oklahoma and another over northern Sonora State, Mexico. By 0600 UTC, the long-wave 500-hPa trough remained roughly over the Rocky Mountain states, and the short-wave troughs seen over northwestern Oklahoma and northern Sonora State at 0000 UTC

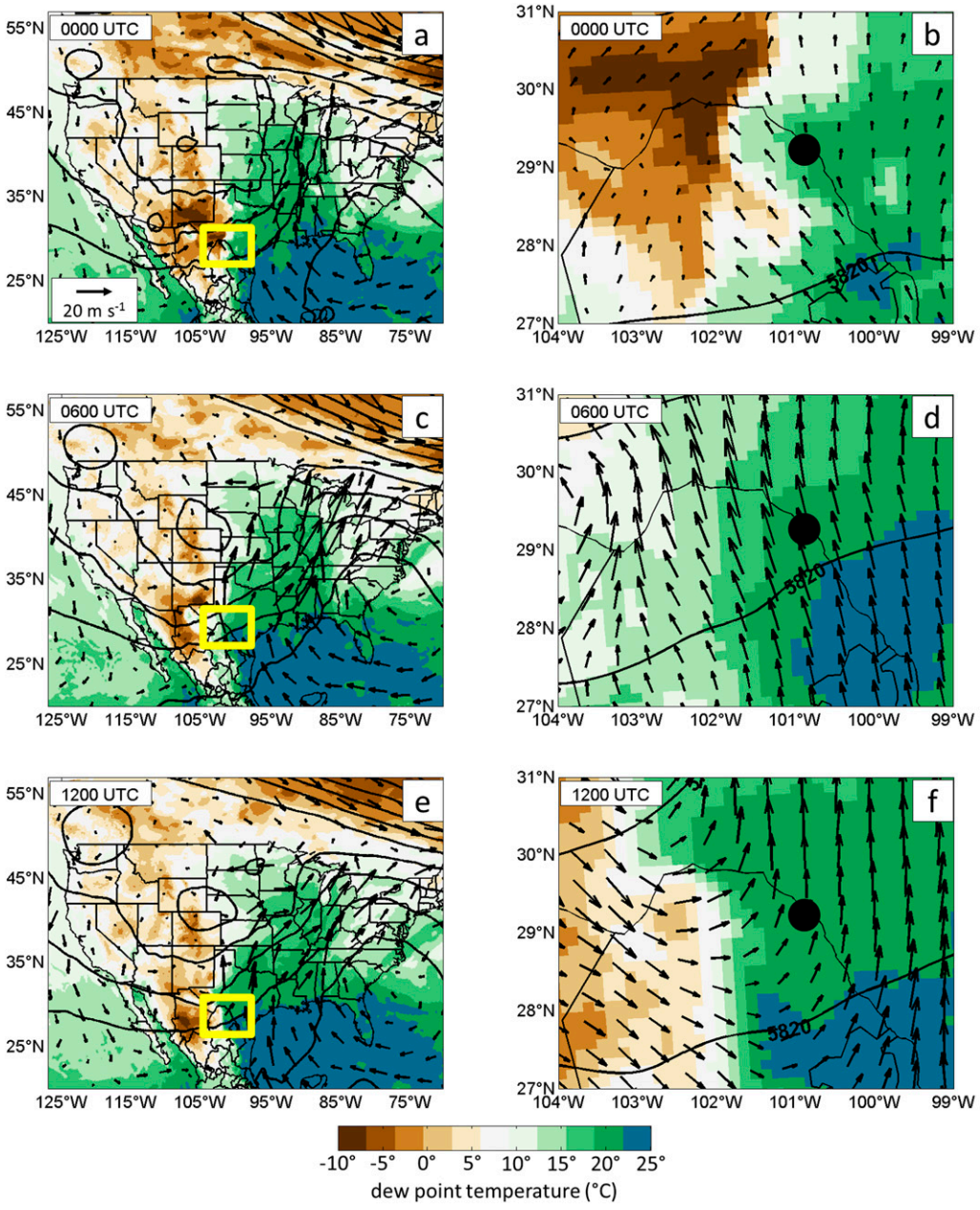

FIG. 7. Height at 500 hPa (black lines, contoured every 60 m starting at 5860 m in lower right), wind at 850 hPa ($m\,s^{-1}$), and 2-m dewpoint temperature (°C) at (a),(b) 0000; (c),(d) 0600; and (e),(f) 1200 UTC 25 May 2015. (b),(d),(f) Images are zoomed to the SdB region, indicated by yellow box in (a),(c), and (e). Position of Ciudad Acuña given by black dot in (b),(d), and (f). Reference wind vector for all panels given in (a). All data from RAP model analyses.

had moved eastward and northeastward and were analyzed over eastern Nebraska and western Chihuahua State, respectively (Fig. 7c). By 1200 UTC, a closed 500-hPa low was analyzed over southeastern Wyoming, northeastern Colorado, and western Nebraska, while the short-wave troughs over eastern Nebraska and western Chihuahua had moved into Iowa and west Texas, respectively (Fig. 7e). The broad synoptic-scale circulation at 850 hPa was cyclonic over the Gulf of Mexico and the adjacent states of Texas, Tamaulipas, Veracruz, and also over Coahuila throughout the 0000–1200 UTC period (Figs. 7a–f) in response to cyclogenesis at 850 hPa (not shown) resulting from the approach of the long-wave trough at 500 hPa. Furthermore, a

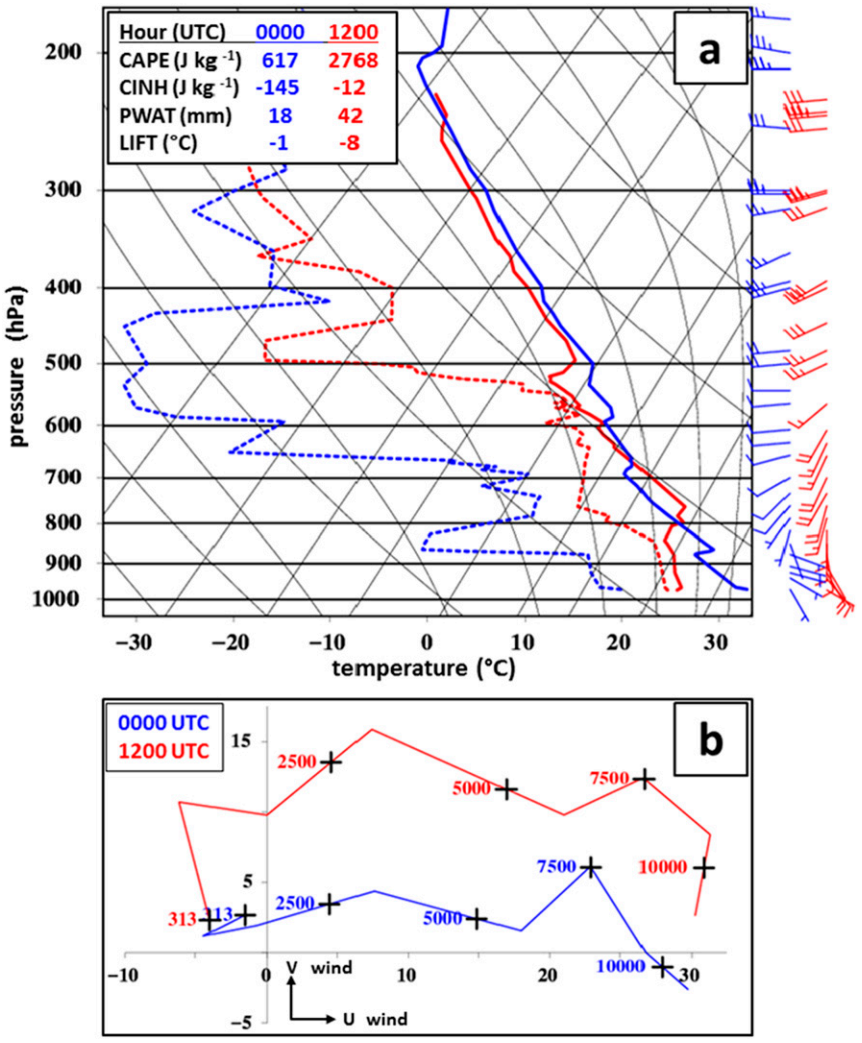

FIG. 8. (a) Radiosonde and (b) hodograph observations from KDRT at 0000 UTC 25 May (blue, 1900 LT 24 May) and 1200 UTC 25 May 2015 (red, 0700 LT 25 May). In (a), solid lines represent air temperature and dashed lines dewpoint temperature. In (a) and (b), wind speeds ($m\,s^{-1}$) are given. Calculated CAPE, CIN, precipitable water (PWAT), and lifted index (LIFT) provided in (a).

synoptic-scale dryline was analyzed in 2-m dewpoint temperatures from far southwest Kansas generally southward into northern Coahuila.

b. Convection environment

Between 0000 and 1200 UTC 25 May 2015, several important changes in both the 850-hPa flow and surface dewpoint temperatures were seen in the vicinity of Ciudad Acuña. We propose that these changes were most likely associated with the movement of the two short-wave troughs mentioned above. At 0000 UTC, the 850-hPa flow near Ciudad Acuña was southerly, likely having responded to height falls associated with the short-wave trough seen at 500 hPa to the northeast of Ciudad Acuña over northwestern Oklahoma (Fig. 7a). Surface (2 m) dewpoint temperatures at 0000 UTC over Ciudad Acuña were between 15° and 17°C in the RAP analysis, but between 0° and 5°C over the SdB (Fig. 7b). Observations at KDRT at 0000 UTC indicated a 2-m dewpoint temperature of 16.1°C (Fig. 8a). Winds in the 0000 UTC KDRT sounding were southerly to southwesterly between 850 and 700 hPa (Figs. 8a and 8b), which agreed with the RAP analysis. By 0600 UTC, the 850-hPa flow had backed to southeasterly over the Ciudad Acuña region, noted in the RAP analysis over the SdB of northern Coahuila (Fig. 7d). This flow backing was likely in response to both height falls associated with the approach of the short-wave trough

over Chihuahua at 0600 UTC (Fig. 7c), lee troughing associated with persistent southwesterly flow at 500 hPa (Bluestein 1993), and diurnal effects (Jiang et al. 2007). Observed 2-m dewpoint temperatures had risen to 19.4°C at KDRT, in good agreement with moistening seen in the RAP analysis (Fig. 7d). Furthermore, the dryline was analyzed at a position approximately 100 km west of its 0000 UTC position, oriented along a south-southwest to north-northeast line west of the SdB (Fig. 7c), with 2-m dewpoint temperatures up to 15°C over the eastern SdB (Fig. 7d). At 1200 UTC, around 30 min after dissipation of the Ciudad Acuña tornado, southerly flow at 850 hPa of approximately 10 m s^{-1} was seen in the RAP analysis (Fig. 7f), in agreement with the KDRT sounding of 850-hPa wind of 9.7 m s^{-1} from 180° (Figs. 8a and 8b).

c. *Forcing for convection initiation*

The synoptic- and mesoscale environment in northern Coahuila on 25 May 2015, characterized by a dryline, significant moistening at the surface, and strengthening low-level flow, has been identified as favorable for supercell and tornado formation (e.g., Bluestein et al. 1989; Hane et al. 1997; Bluestein 2009; Hane et al. 2001). However, to realize those favorable conditions, a storm must have initiated. Observations from the KDFX radar indicated two instances of convection initiation in the early morning hours of 25 May 2015, one at 0628 UTC (0128 LT) and another at 0728 UTC (0228 LT). The second instance went on to produce the tornadic supercell that affected Ciudad Acuña. No other thunderstorms formed in northern Coahuila from 0600 to 1200 UTC, and both instances of convection initiation occurred in the center of the SdB, suggesting the importance of the mountains to convection initiation. It is important to note that convection initiation in persistent upslope flow remains a complex process, as noted by the modeling results in Weckwerth et al. (2014). It is likely that in this case, the combination of surface upslope flow, moisture return to the elevated terrain, and synoptic-scale forcing from the approaching short-wave trough all contributed to the initiation of overnight convection. Forcing from surface upslope flow and horizontal mass convergence as a result of synoptic-scale flow is investigated in this section.

To better examine the physical forcing mechanisms responsible for initiation in this case, hourly fields of both upslope flow and horizontal surface mass convergence were examined. At 0600 UTC 25 May 2015, upslope surface flow was noted over much of northern Coahuila and southern Texas (Fig. 9a), a result of the increase in terrain height from southeast to northwest and the synoptic-scale southeasterly surface flow. Upslope flow was maximized on the southeastward-facing sides of the topography of the SdB, a result of the southeasterly surface flow impinging on the mountains (Fig. 9a). Between 0600 and 0700 UTC, the first of two thunderstorms formed over the northernmost SdB (near 28.8°N, 102°W), with base reflectivity echoes of 20 dBZ seen from KDFX radar at 0628 UTC. At 0700 UTC, the pattern of upslope flow remained largely unchanged from 0600 UTC, with the largest values of upslope flow centered along the southeastward-facing slopes of the SdB (Fig. 9b). The largest values of negative (downslope) flow were seen at both hours on the northwestward-facing slopes of the SdB. At 0800 UTC, upslope flow was still present, maximized over the peaks of the SdB (Fig. 9c). The second instance of convection initiation occurred at 0728 UTC near 28.5°N, 102.4°W, also over a region of persistent positive upslope flow. From 0900 to 1100 UTC (Figs. 9d–f), upslope flow remained positive over the SdB peaks, generally weakened over the eastern sloping plains at 0900 and 1000 UTC as wind speeds diminished during those 2 hours (Figs. 9d and 9e), and then strengthened again over the eastern plains at 1100 UTC as wind speeds strengthened (Fig. 9f). This mesoscale pattern suggests that both instances of convection initiation in the SdB between 0600 and 0800 UTC 25 May 2015 were tied to upslope flow. It also suggests that once formed, both storms moved east-northeastward through an area characterized by upslope flow.

RAP analyses of horizontal surface mass convergence indicated that the SdB region at 0600 UTC was generally characterized by surface mass divergence (Fig. 10a), with the largest divergence centered near the SdB peaks. This general divergence pattern persisted at 0700 (Fig. 10b) and 0800 UTC (Fig. 10c). By 0900 and 1000 UTC, horizontal mass convergence was seen in the eastern plains to the southeast of the SdB (Figs. 10d and 10e), but 100 km to the southeast of the developing thunderstorm. Thus, while the contribution from surface horizontal mass divergence is less clear, persistent surface upslope flow over the elevated terrain of the SdB did appear to be a contributing factor in allowing parcels to reach their level of free convection and initiate convection.

d. *Storm environment*

The mesoscale thermodynamic and dynamic environments reflected conditions known to be favorable for supercell development and tornadogenesis. For example, from 0600 to 1100 UTC 25 May 2015, surface-based CAPE values from the RAP analyses increased from below 1000 to above 4000 J kg^{-1}, and surface-based CIN values decreased from near −100 J kg^{-1} to

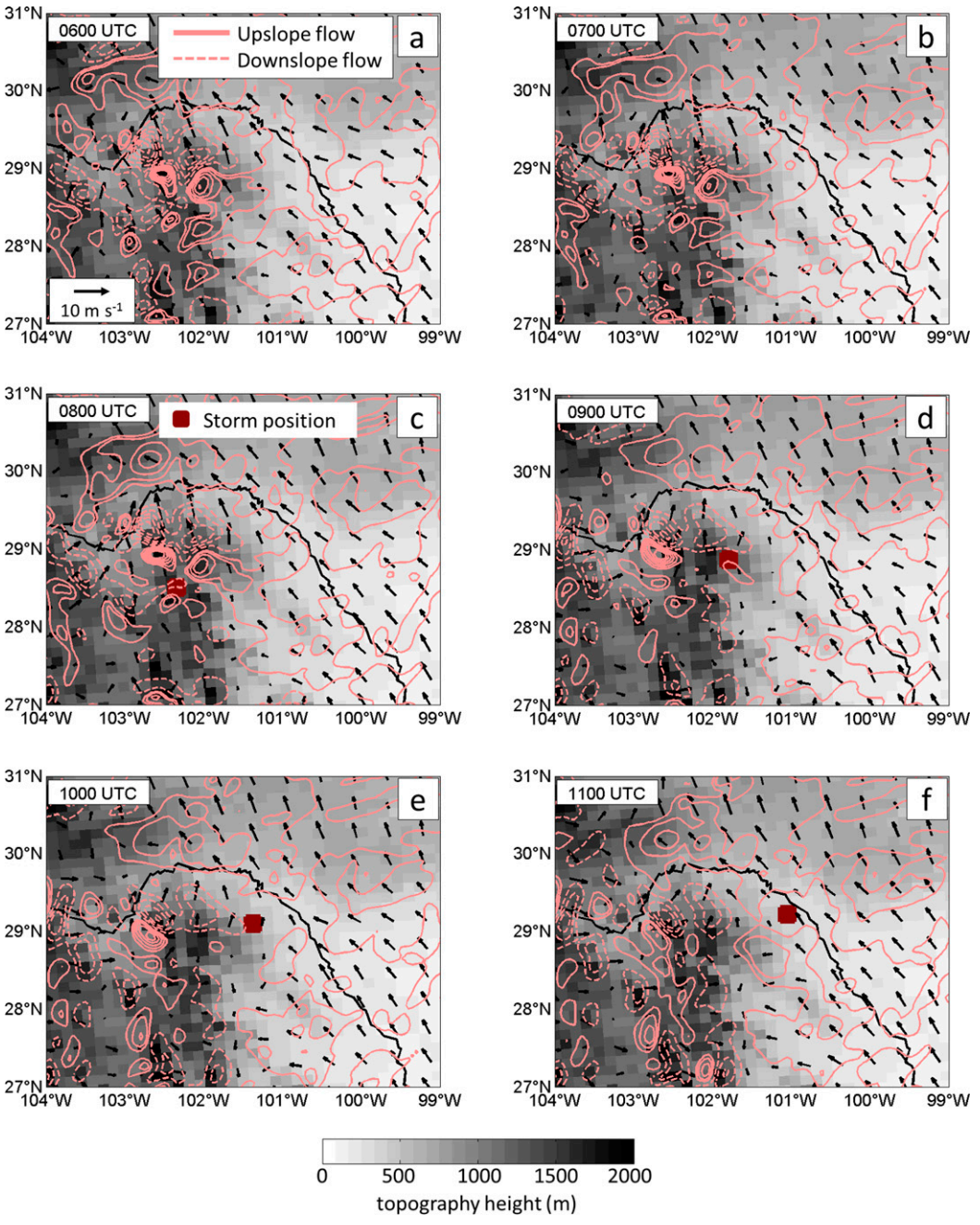

FIG. 9. Topography height (grayscale, m), 10-m wind (vector, m s^{-1}), and 10-m upslope flow component (positive in solid pink; negative in dashed pink; interval: 0.05 m s^{-1}) for (a)–(f) 0600–1100 UTC 25 May 2015 from RAP model analyses. Radar-based storm position at each hour indicated by dark red circle. Reference wind vector given in (a).

near zero (Figs. 11a–f). Values of 0–1-km SRH (Davies and Johns 1993; Markowski et al. 1998) generally weakened between 0600 and 1100 UTC (Figs. 11a–f). For example, at 0600 UTC, values of 0–1 km SRH were between 250 and 300 $m^2 s^{-2}$ over the SdB (Fig. 11a) but decreased to around 150 $m^2 s^{-2}$ by 1100 UTC to the east of the SdB (Fig. 11f). These RAP-based values at 1100 UTC were comparable to the values calculated from the observed wind profile from the 1200 UTC KDRT radiosonde (Figs. 8a,b) using a storm motion out of 250° at 18 kt (motion parameters calculated by visually estimating positions of the hook portion of the supercell in base reflectivity observations from the KDFX radar). From the 1200 UTC 25 May 2015 KDRT

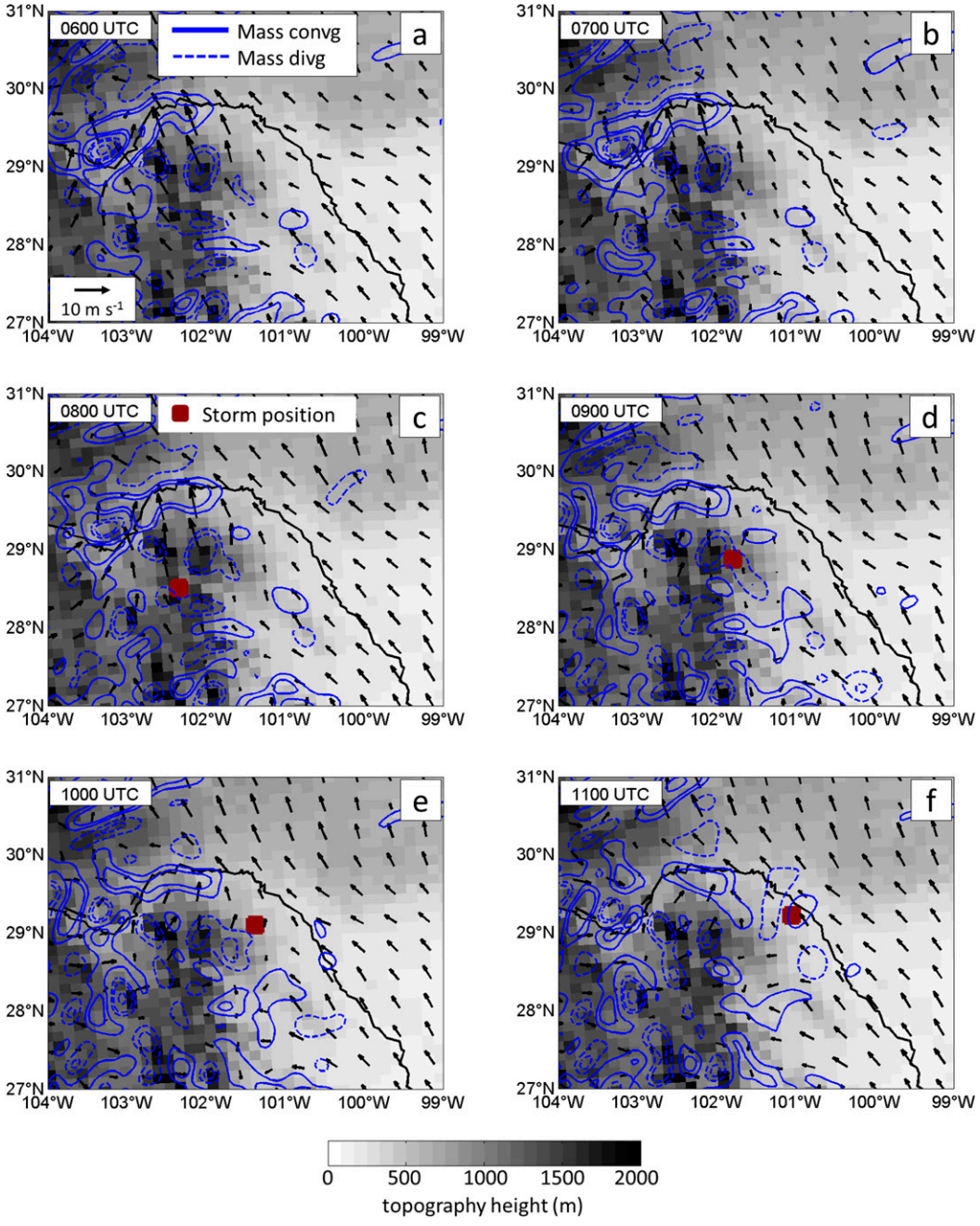

FIG. 10. As in Fig. 9, but blue solid (dashed) contours indicate horizontal mass convergence (divergence) at 10 m, with data from RAP model analyses. Contour interval is every 2×10^{-4} kg m^{-3} s^{-1}. Radar-based storm position at 0800–1100 UTC indicated by dark red circle. Reference wind vector given in (a).

radiosonde, observed 0–1-km SRH was 158 m^2 s^{-2}, 0–3-km SRH was 309 m^2 s^{-2}, and 0–6-km bulk wind difference was 56 kt (Fig. 8). These combinations of CAPE, CIN, helicity, and wind shear put the environment of the Ciudad Acuña tornado event in the middle to upper ranges of phase–space combinations in the climatological studies of Rasmussen and Blanchard (1998), Thompson et al. (2003), Rasmussen (2003), and Potvin et al. (2010). They also agree with the daytime environments favoring supercellular convection found by E06 and WZ08.

From 0000 to 0600 UTC, surface flow in the SdB near 28.5°N, 102.4°W was upslope (Fig. 12a). Surface-based CAPE values increased from near zero to near 1500 J kg^{-1}, while surface-based CIN remained steady

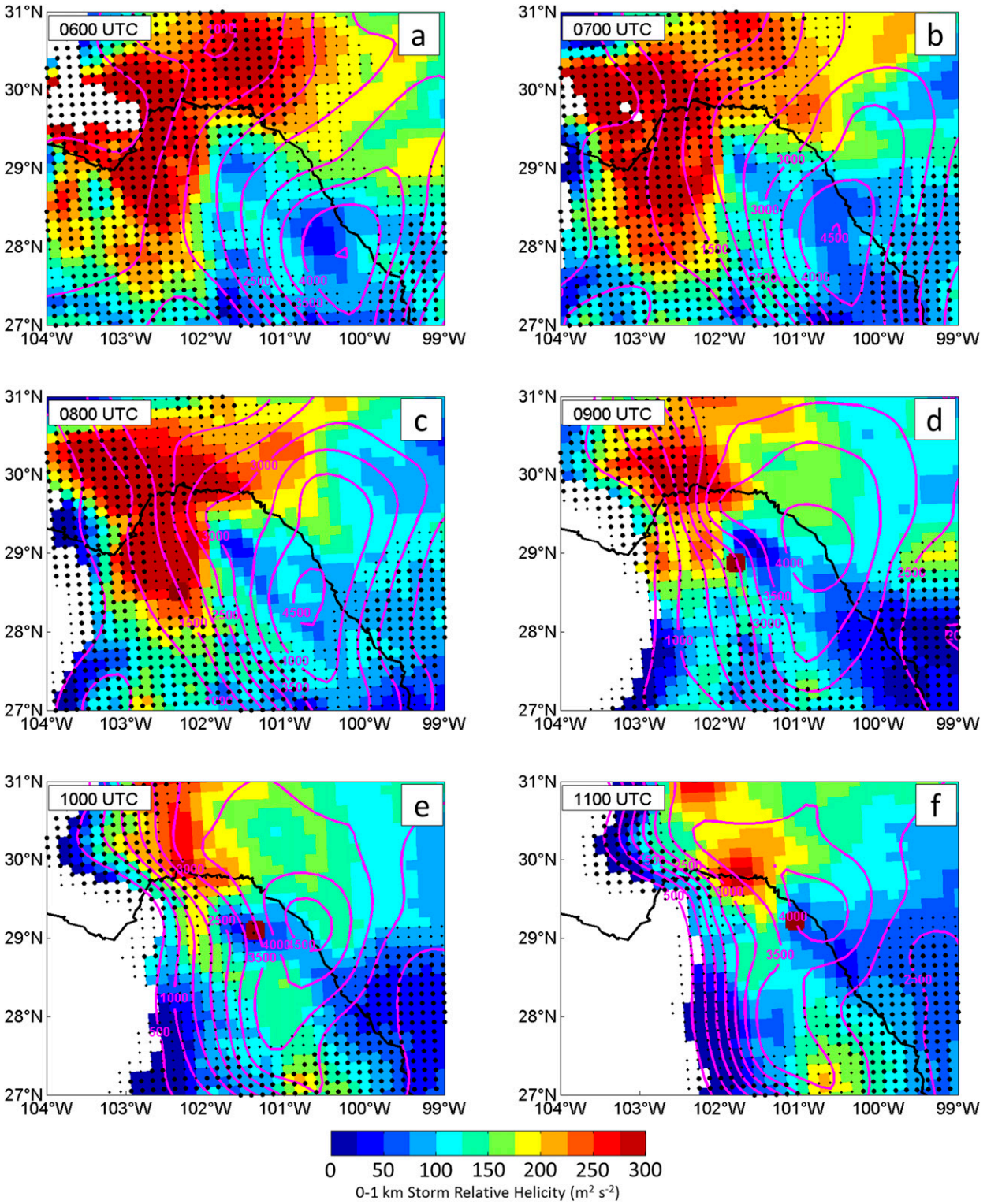

FIG. 11. CAPE (magenta contours every 500 J kg^{-1}), 0–1-km SRH (shaded, m^2 s^{-2}), and CIN (large dots indicate CIN < -100 J kg^{-1}; small dots indicate CIN between -50 and -100 J kg^{-1}; no dots indicate CIN > -50 J kg^{-1}) for (a)–(f) 0600–1100 UTC 25 May 2015. SRH is contoured only where CAPE is positive. All data from RAP model analyses. Radar-based storm position at each hour indicated by dark red circle.

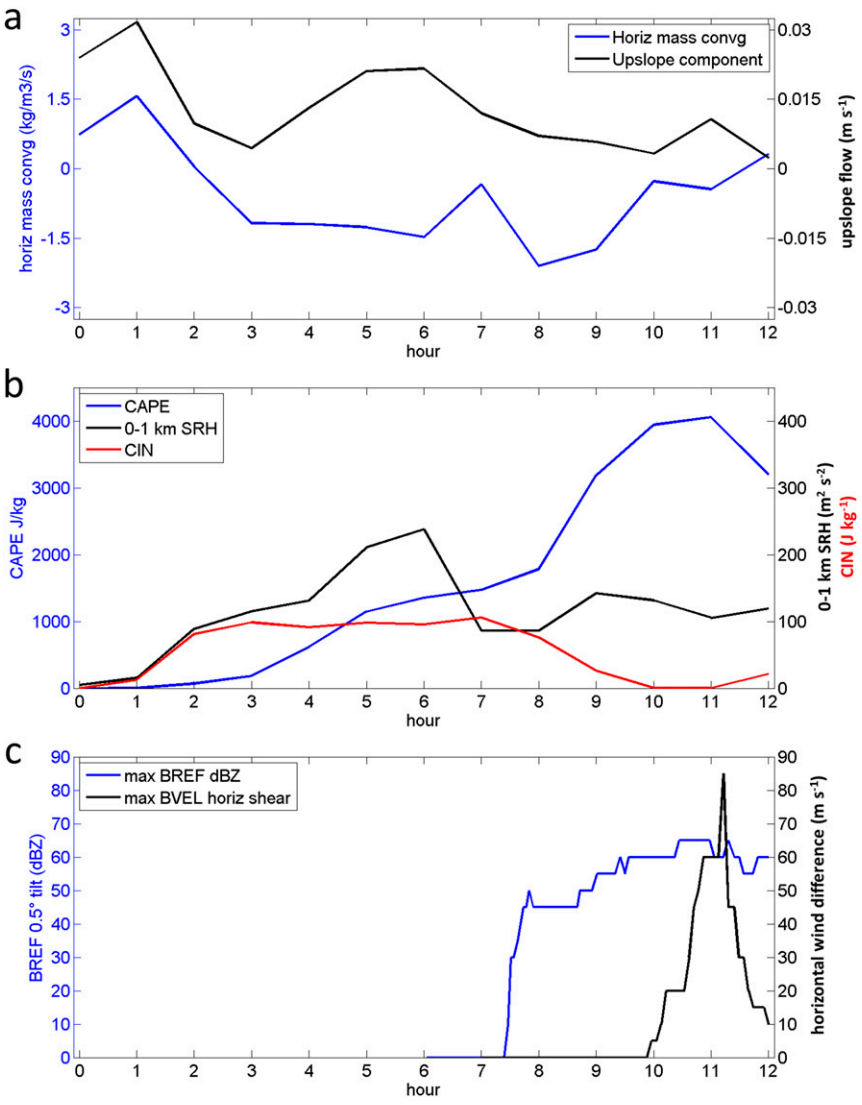

FIG. 12. (a) Upslope flow component at 10 m (black curve; $m\,s^{-1}$) and horizontal mass convergence (blue curve; $kg\,m^{-3}\,s^{-1}$). (b) CAPE (blue curve; $J\,kg^{-1}$), 0–1-km SRH (black curve; $m^2\,s^{-2}$), and CIN (red curve; $J\,kg^{-1}$). (c) Highest base reflectivity (blue curve; dBZ) and horizontal wind difference (black curve; $m\,s^{-1}$). All data from RAP model analyses. From 0000 to 0700 UTC 25 May 2015, all values are for the nine RAP model grid points closest to the point of CIN at 0728 UTC. From 0800 to 1200 UTC 25 May 2015, all values are for the nine RAP model grid points 25 km (two grid points) to the southeast of the thunderstorm location.

near $-100\,J\,kg^{-1}$. Once the thunderstorm formed (at 0728 UTC), CAPE values increased along its trajectory from about $1500\,J\,kg^{-1}$ at 0800 UTC to over $3500\,J\,kg^{-1}$ at 1100 UTC (Fig. 12b). Meanwhile, horizontal mass convergence increased to near zero (Fig. 12a). From 0600 to 1100 UTC, 0–1-km SRH remained relatively constant near $150\,m^2\,s^{-2}$ (Fig. 12b). The increase in CAPE and the decrease in CIN from 0900 to 1100 UTC occurred concurrently with an increase observed in radar reflectivity (from 45 to 65 dBZ), and especially with an observed increase in radial wind difference, from near $0\,m\,s^{-1}$ at 0900 to $85\,m\,s^{-1}$ at 1113 UTC (Fig. 12c). It is clear that once the thunderstorm initiated, it moved into a thermodynamic and kinematic environment very favorable for strengthening. Results of simulations exploring the effects of the SdB topography on storm initiation are presented in the next section.

5. WRF Model results: Sensitivity to topography

The previous sections discussed the evolution of a supercell thunderstorm in observations from the KDFX

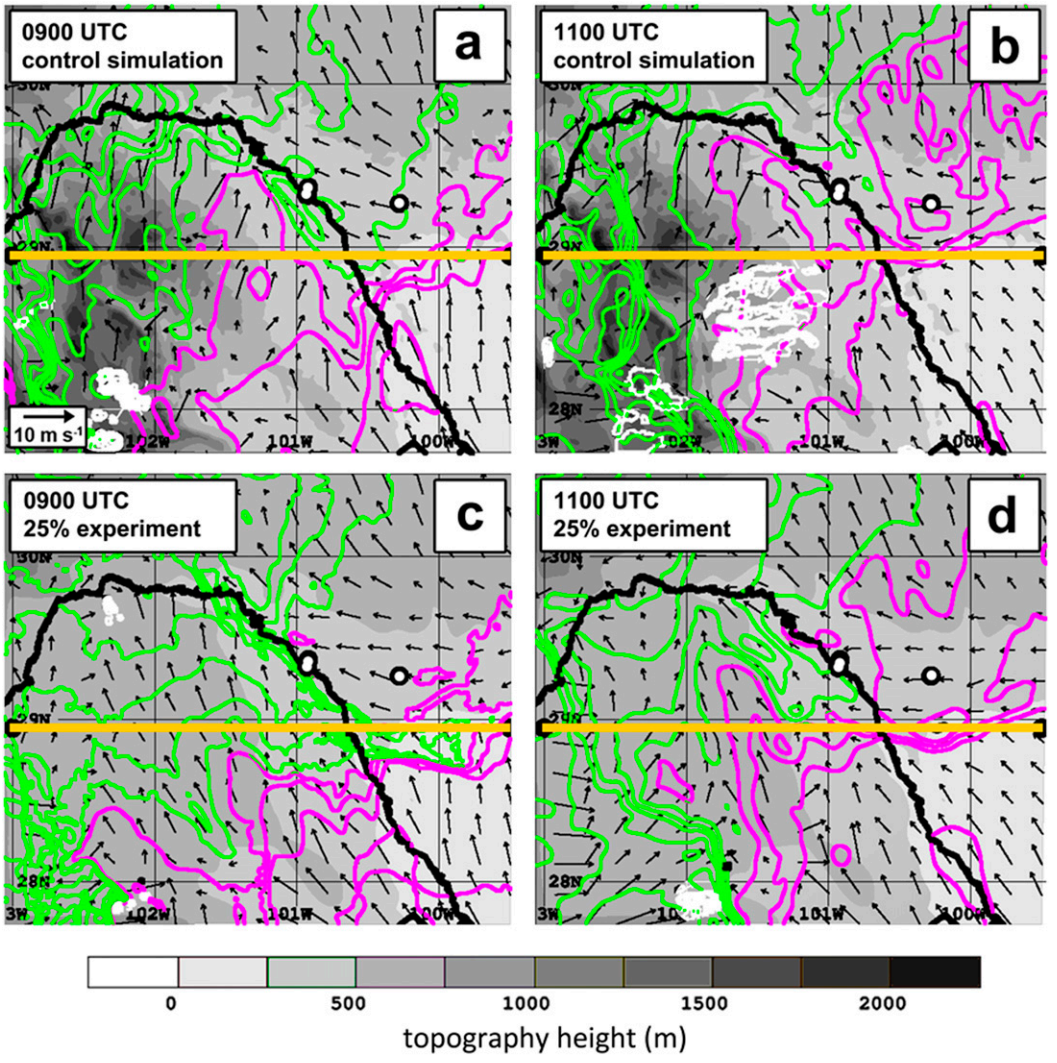

FIG. 13. Dewpoint temperature at 2 m (green and magenta lines, °C) and 10-m horizontal wind vectors from 1-km WRF Model simulations initialized at 0000 UTC 24 May 2015. Gray shading represents topography height (m). Light green lines correspond to dewpoint temperatures from 0° to 12.5°C. Magenta lines correspond to dewpoint temperatures from 15° to 22.5°C. Both light green and magenta lines are spaced at 2.5°C intervals. White contours are radar reflectivity every 10 dB*Z*. Positions of Ciudad Acuña, the Del Rio upper-air site, and the KDFX radar are indicated by small circles. Vertical cross sections presented in Fig. 15 are indicated by orange lines.

radar and in synoptic-scale and mesoscale circulations from RAP gridded analyses. From those analyses, surface upslope flow emerged as a primary candidate to explain convection initiation over the SdB. To further explore the role of topography in initiating the thunderstorm that eventually produced the Ciudad Acuña tornado, four high-resolution WRF simulations with different topography were performed. The 100% (control), 75%, and 50% topography sensitivity experiments yielded similar results: all featured convection initiation between 0800 and 0900 UTC about 10–20 km to the east of a maximum in upslope flow in the south-central SdB near 28°N. In those three simulations, convection initiated about 100 km south of the observed area of convection initiation. Furthermore, all three simulations sustained the convection as it propagated to the east, reaching the U.S.–Mexico border between 1100 and 1300 UTC. Because of their similarity, only one of the three, the control run, will be compared to the 25% topography simulation.

In the 1-km domain of the control simulation, southerly to south-southwesterly surface winds and dewpoint temperatures between 10° and 15°C were present over the SdB at 0900 UTC 25 May 2015 (Fig. 13a). At that time, two clusters of thunderstorms were noted in WRF radar base reflectivity fields near 28°N, 102.3°W, in a

region of positive upslope flow and near-zero horizontal mass convergence, similar to the RAP analyses (not shown). Those simulated thunderstorms moved east-northeastward and at 1100 UTC were located between 28.5° and 29°N, 101.8° and 101.2°W in a region of southwesterly surface winds and surface dewpoint temperatures between 15° and 20°C (Fig. 13b). In the 1-km domain of the simulation with the SdB topography reduced to 25%, surface flow at 0900 UTC was southeasterly over the entire SdB region, and dewpoint temperatures ranged from 10° to 22°C, with highest values in the southeast and lowest values in the southwest of the domain (Fig. 13c). The greatest dewpoint temperature gradient, likely associated with the dryline, was seen in the southwest portion of the domain. Only two small regions of convection activity were noted: one in the extreme north of Coahuila near 29.8°N, 102.3°W and one in the southwest of the domain, near the dryline at 27.9°N, 102.1°W (Fig. 13c). By 1100 UTC, surface flow was southeasterly over about the eastern two-thirds of the simulation domain (Fig. 13d), while dewpoint temperatures remained between 15° and 22°C in the border region but had decreased to below 10°C in the southwestern portion of the domain, to the west of the dryline. The northern convection activity had dissipated, while the southern activity moved only 25 km to the east, to near 27.9°N, 101.9°W. Swaths of cumulative radar reflectivity from 0600 to 1200 UTC (Fig. 14) confirmed that storms formed in the southern SdB in the control experiment and propagated northeastward (Fig. 14a), while very little reflectivity and almost no propagation was seen in the 25% experiment (Fig. 14b).

A vertical cross section through the center of the SdB revealed that, at 0900 UTC, lower-tropospheric mixing ratio values in the eastern plains were higher in the control experiment (Fig. 15a) than in the 25% experiment (Fig. 15c). Over the SdB region, mixing ratio values were 2–4 $g\,kg^{-1}$ smaller in the control experiment than in the 25% experiment, likely the result of greater westward transport of moisture in the 25% experiment due to the absence of blocking topography. Upward vertical motion of -5 to $-10\,Pa\,s^{-1}$ (approximately 0.5–1.0 $m\,s^{-1}$) in the control experiment occurred throughout the lower and midtroposphere (850–400 hPa) over the SdB (Fig. 15a), but very little upward motion occurred in the 25% experiment (Fig. 15c). By 1100 UTC, the dryline was located just east of the SdB in both experiments, with very similar mixing ratio values in both experiments (Figs. 15b and 15d). However, again upward vertical motion of -5 to $-15\,Pa\,s^{-1}$ (approximately 0.5–1.5 $m\,s^{-1}$) occurred over much of the SdB in the control experiment (Fig. 15b), while very little upward vertical motion occurred in the 25% experiment (Fig. 15d).

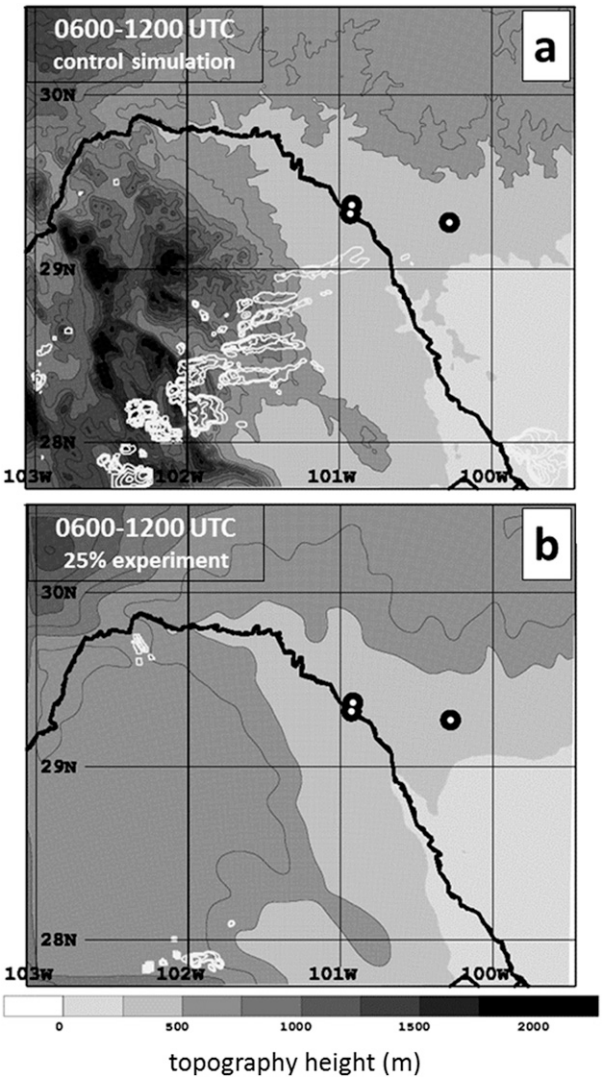

FIG. 14. Cumulative radar reflectivity swaths (white contours, every 10 dBZ) from 0600 to 1200 UTC 25 May 2015 for (a) control simulation with 100% topography and (b) experiment with 25% topography. Gray shading indicates topography height (m).

The differences between the evolution of both the radar reflectivity (Fig. 14) and vertical velocity (Fig. 15) fields between the control and 25% experiments show the importance of the SdB topography to both the initiation and the maintenance of deep convection. In the control experiment, two convective clusters initiated over two different SdB peaks, the northernmost one over 50 km to the east of the dryline, in areas of upslope flow. In the 25% topography experiment, weaker convection developed right at the dryline in the absence of surface upslope flow. In the control one, the convection propagated well east of the SdB and remained between 50 and 100 km to the east of the dryline. With reduced elevations, the

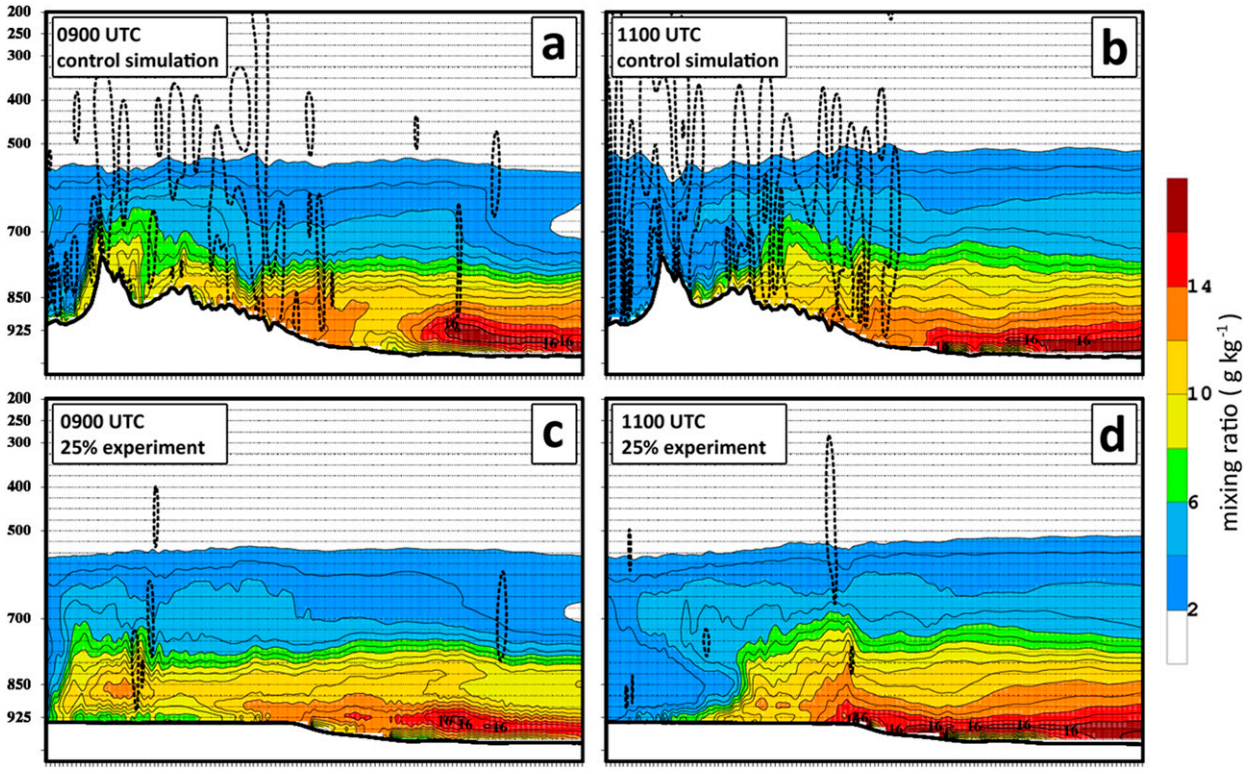

FIG. 15. Cross sections of mixing ratio (shaded, g kg^{-1}) and upward vertical velocity (dashed contours every 5 Pa s^{-1}, corresponding to every 0.5 m s^{-1}) from 1-km WRF simulations with (a),(b) 100% topography and (c),(d) elevations reduced to 25%. Sections are along 28.95°N, from 102.95° through 99.55°W, as indicated by orange lines in Fig. 13.

convection moved only 25 km in 2 hours and remained located near the dryline.

Combining the output of these simulations with the RAP analyses, it is clear that upslope flow played a role in initiating and sustaining convection in the SdB. In the presence of topography, convection initiation occurred in regions of upslope flow over the tallest SdB peaks, approximately 100 km to the east of the dryline. Storms then moved east through a region of continued upslope flow, into an environment progressively more favorable for intensification. In the absence of mountains, weak storms did initiate along the dryline, likely in response to a combination of mesoscale forcing from the dryline circulation and synoptic-scale forcing from the approaching short-wave trough over Chihuahua, but those storms were not sustained nor did they exhibit eastward propagation.

6. Discussion and conclusions

The tornado that affected Ciudad Acuña during the early morning hours (1045–1130 UTC) of 25 May 2015 was studied using observations, gridded analyses, and results from sensitivity experiments from a numerical model. The synoptic-scale environment from 0000 to 1200 UTC showed a long-wave trough at 500 hPa over the western United States and Mexico that slowly progressed eastward. In this long-wave trough, two short-wave troughs were analyzed: one over northwestern Oklahoma at 0000 UTC and another over Sonora State, Mexico, at 0000 UTC. As a result of height falls associated with the Oklahoma short-wave trough, low-level flow over Coahuila State was southerly to south-southwesterly at 0000 UTC. The combined effects of a short-wave trough moving into northern Chihuahua and diurnal effects led the low-level flow to back to the southeast, transporting rich low-level moisture onto the SdB. This southeasterly flow had a surface upslope component over the SdB. Convection initiation occurred around 0628 UTC, and by 0900 UTC discrete thunderstorms evident from the KDFX radar were moving eastward off the SdB and into the highly unstable (CAPE above 3000 J kg^{-1}) and highly sheared (0–6-km bulk wind difference over 50 kt) atmosphere in the vicinity of Ciudad Acuña. The evolution of the second of those storms in base reflectivity radar imagery confirmed its evolution into a supercell, including developing a hook echo, by 1040 UTC.

Convective activity over the SdB has received attention in other studies (e.g., E06 and WZ08). However, those studies focused on daytime convection where elevated heating on the peaks of the SdB would drive upslope convergent surface flow and serve as the primary mechanisms for afternoon convection initiation. Here, we have shown that nocturnal upslope flow, when combined with an otherwise favorable synoptic-scale environment, can contribute to initiation of deep convection over the SdB. Both RAP analyses and WRF simulations indicated that upslope flow was present over the peaks of the central SdB at the hour of initiation. Combined with the approach of a short-wave trough from the west, this environment proved favorable for initiation where upslope flow was maximized. A dryline, located 50–100 km to the west of the location of convection initiation in the RAP analyses and WRF control simulation, did not appear to factor into convection initiation. However, in the WRF simulation with reduced (25%) elevations, two small regions of convection initiation were noted. The inability for the convection, in this simulation, to sustain itself or to propagate eastward suggested that the continued upslope flow environment from 0600 to 1000 UTC was important in maintaining the nocturnal convection while it propagated into the plains east of the SdB. Once it reached the eastern plains, CAPE values rapidly increased to over 3500 J kg^{-1} and CIN decreased to near zero, providing thermodynamical support to intensify the convection.

Based on these results, we encourage Civil Defense Agency authorities and operational forecasters in Coahuila and elsewhere to be aware of the potential for convection initiation in the SdB during the overnight and early morning hours, particularly for events that feature synoptic-scale upslope (southeasterly) surface flow. The upslope flow, combined with large-scale ascent favoring convection associated with the approach of a short-wave trough (Bluestein 1993), can result in convection initiation over the SdB in the absence of daytime heating and surface horizontal mass convergence, which are mechanisms that have been more traditionally associated with convection initiation in the region.

Acknowledgments. The authors thank J. Delgado Jiménez, who provided technical assistance with the WRF Model simulations at CICESE's computing facility in Ensenada; and I. Villanueva, who provided technical assistance with figure creation. The authors also wish to thank the World Wide Lightning Location Network (http://wwlln.net), a collaboration among over 50 universities and institutions, for providing the lightning location data used in this paper. B.S.B. acknowledges the support of the Fulbright Scholar program and DGAPA-UNAM during the academic visit to UNAM. This study was partially funded by the PAPIIT program under Grant IN-104416 and by the Academic Mobility program at UNAM. Finally, the authors thank the three anonymous reviewers for their helpful comments, which resulted in an improved manuscript.

REFERENCES

Ashley, W. S., 2007: Spatial and temporal analysis of tornado fatalities in the United States, 1880–2005. *Wea. Forecasting*, **22**, 1214–1228, doi:10.1175/2007WAF2007004.1.

——, A. J. Krmenec, and R. Schwantes, 2008: Vulnerability due to nocturnal tornadoes. *Wea. Forecasting*, **23**, 795–807, doi:10.1175/2008WAF2222132.1.

Banacos, P. C., and D. M. Schultz, 2005: The use of moisture flux convergence in forecasting convective initiation: Historical and operational perspectives. *Wea. Forecasting*, **20**, 351–366, doi:10.1175/WAF858.1.

Barrett, B. S., R. Garreaud, and M. Falvey, 2009: Effect of the Andes Cordillera on precipitation from a midlatitude cold front. *Mon. Wea. Rev.*, **137**, 3092–3109, doi:10.1175/2009MWR2881.1.

Barthlott, C., U. Corsmeier, C. Meißner, F. Braun, and C. Kottmeier, 2006: The influence of mesoscale circulation systems on triggering convective cells over complex terrain. *Atmos. Res.*, **81**, 150–175, doi:10.1016/j.atmosres.2005.11.010.

Benjamin, S. G., and Coauthors, 2006: From the 13-km RUC to the Rapid Refresh. *12th Conf. on Aviation Range and Aerospace Meteorology*, Atlanta, GA, Amer. Meteor. Soc., 9.1. [Available online at https://ams.confex.com/ams/Annual2006/techprogram/paper_104851.htm.]

Bluestein, H. B., 1993: *Observations and Theory of Weather Systems*. Vol. II, *Synoptic-Dynamic Meteorology in Midlatitudes*, Oxford University Press, 608 pp.

——, 2000: A tornadic supercell over elevated, complex terrain: The Divide, Colorado, storm of 12 July 1996. *Mon. Wea. Rev.*, **128**, 795–809, doi:10.1175/1520-0493(2000)128<0795:ATSOEC>2.0.CO;2.

——, 2009: The formation and early evolution of the Greensburg, Kansas, tornadic supercell on 4 May 2007. *Wea. Forecasting*, **24**, 899–920, doi:10.1175/2009WAF2222206.1.

——, E. W. McCaul Jr., G. P. Byrd, G. R. Woodall, G. Martin, S. Keighton, and L. C. Showell, 1989: Mobile sounding observations of a thunderstorm near the dryline: The Gruver, Texas storm complex of 25 May 1987. *Mon. Wea. Rev.*, **117**, 244–250, doi:10.1175/1520-0493(1989)117<0244:MSOOAT>2.0.CO;2.

Bonner, W. D., 1968: Climatology of the low-level jet. *Mon. Wea. Rev.*, **96**, 833–850, doi:10.1175/1520-0493(1968)096<0833:COTLLJ>2.0.CO;2.

Brooks, H. B., C. A. Doswell III, and J. Cooper, 1994: On the environments of tornadic and nontornadic mesocyclones. *Wea. Forecasting*, **9**, 606–618, doi:10.1175/1520-0434(1994)009<0606:OTEOTA>2.0.CO;2.

Burgess, D. W., V. T. Wood, and R. A. Brown, 1982: Mesocyclone evolution statistics. Preprints, *12th Conf. on Severe Local Storms*, San Antonio, TX, Amer. Meteor. Soc., 422–424.

Chen, F., and J. Dudhia, 2001: Coupling an advanced land surface–hydrology model with the Penn State–NCAR MM5 modeling system. Part I: Model implementation and sensitivity. *Mon.*

Wea. Rev., **129**, 569–585, doi:10.1175/1520-0493(2001)129<0569:CAALSH>2.0.CO;2.

Chen, T.-C., and J. A. Kpaeyeh, 1993: The synoptic-scale environment associated with the low-level jet of the Great Plains. *Mon. Wea. Rev.*, **121**, 416–420, doi:10.1175/1520-0493(1993)121<0416:TSSEAW>2.0.CO;2.

Chu, C.-M., and Y.-L. Lin, 2000: Effects of orography on the generation and propagation of mesoscale convective systems in a two-dimensional conditionally unstable flow. *J. Atmos. Sci.*, **57**, 3817–3837, doi:10.1175/1520-0469(2001)057<3817:EOOOTG>2.0.CO;2.

Davies, J. M., and R. H. Johns, 1993: Some wind and instability parameters associated with strong and violent tornadoes: 1. Wind shear and helicity. *The Tornado: Its Structure, Dynamics, Prediction, and Hazards*, *Geophys. Monogr.*, Vol. 79, Amer. Geophys. Union, 573–582.

——, and A. Fischer, 2009: Environmental characteristics associated with nighttime tornadoes. *Electron. J. Oper. Meteor.*, **10** (3). [Available online at http://nwafiles.nwas.org/ej/pdf/2009-EJ3.pdf.]

Deierling, W., and W. A. Peterson, 2008: Total lightning activity as an indicator of updraft characteristics. *J. Geophys. Res.*, **113**, D16210, doi:10.1029/2007JD009598.

Doswell, C. A., III, H. E. Brooks, and N. Dotzek, 2009: On the implementation of the enhanced Fujita scale in the USA. *Atmos. Res.*, **93**, 554–563, doi:10.1016/j.atmosres.2008.11.003.

Dudhia, J., 1989: Numerical study of convection observed during the winter monsoon experiment using a mesoscale two-dimensional model. *J. Atmos. Sci.*, **46**, 3077–3107, doi:10.1175/1520-0469(1989)046<3077:NSOCOD>2.0.CO;2.

Dunn, L. B., and S. V. Vasiloff, 2001: Tornadogenesis and operational consideration of the 11 August 1999 Salt Lake City tornado as seen from two different Doppler radars. *Wea. Forecasting*, **16**, 377–398, doi:10.1175/1520-0434(2001)016<0377:TAOCOT>2.0.CO;2.

Edwards, R., 2006: Supercells of the Serranías del Burro (Mexico). *23rd Conf. on Severe Local Storms*, St. Louis, MO, Amer. Meteor. Soc., P6.2. [Available online at https://ams.confex.com/ams/23SLS/techprogram/paper_114980.htm.]

Fawbush, E., and R. Miller, 1952: A mean sounding representative of the tornadic airmass environment. *Bull. Amer. Meteor. Soc.*, **33**, 303–307.

Forbes, G. S., 1981: On the reliability of hook echoes as tornado indicators. *Mon. Wea. Rev.*, **109**, 1457–1466, doi:10.1175/1520-0493(1981)109<1457:OTROHE>2.0.CO;2.

Fujita, T. T., 1965: Formation and steering mechanisms of tornado cyclones and associated hook echoes. *Mon. Wea. Rev.*, **93**, 67–78, doi:10.1175/1520-0493(1965)093<0067:FASMOT>2.3.CO;2.

Fulton, R. A., J. P. Breidenbach, D. Seo, and D. A. Miller, 1998: The WSR-88D rainfall algorithm. *Wea. Forecasting*, **13**, 377–395, doi:10.1175/1520-0434(1998)013<0377:TWRA>2.0.CO;2.

Grell, G. A., and D. Devenyi, 2002: A generalized approach to parameterizing convection combining ensemble and data assimilation techniques. *Geophys. Res. Lett.*, **29**, 1693, doi:10.1029/2002GL015311.

Hane, C. E., H. B. Bluestein, T. M. Crawford, M. E. Baldwin, and R. M. Rabin, 1997: Severe thunderstorm development in relation to along-dryline variability: A case study. *Mon. Wea. Rev.*, **125**, 231–251, doi:10.1175/1520-0493(1997)125<0231:STDIRT>2.0.CO;2.

——, M. E. Baldwin, H. B. Bluestein, T. M. Crawford, and R. M. Rabin, 2001: A case study of severe storm development along a dryline within a synoptically active environment. Part I: Dryline motion and an Eta model forecast. *Mon. Wea. Rev.*, **129**, 2183–2204, doi:10.1175/1520-0493(2001)129<2183:ACSOSS>2.0.CO;2.

Hong, S.-Y., Y. Noh, and J. Dudhia, 2006: A new vertical diffusion package with an explicit treatment of entrainment processes. *Mon. Wea. Rev.*, **134**, 2318–2341, doi:10.1175/MWR3199.1.

Houze, R. A., Jr., 1993: *Cloud Dynamics*. International Geophysics Series, Vol. 53, Academic Press, 573 pp.

Jiang, X., N.-C. Lau, I. Held, and J. Ploshay, 2007: Mechanisms of the Great Plains low-level jet as simulated in an AGCM. *J. Atmos. Sci.*, **64**, 532–547, doi:10.1175/JAS3847.1.

Kingfield, D. M., and J. G. LaDue, 2015: The relationship between automated low-level velocity calculations from the WSR-88D and maximum tornado intensity determined from damage surveys. *Wea. Forecasting*, **30**, 1125–1139, doi:10.1175/WAF-D-14-00096.1.

Kis, A. K., and J. M. Straka, 2010: Nocturnal tornado climatology. *Wea. Forecasting*, **25**, 545–561, doi:10.1175/2009WAF2222294.1.

Lay, E. H., R. H. Holsworth, C. J. Rodger, J. N. Thomas, O. Pinto Jr., and R. L. Dowden, 2004: WWLL global lightning detection system: Regional validation study in Brazil. *Geophys. Res. Lett.*, **31**, L03102, doi:10.1029/2003GL018882.

Lin, Y.-L., 1993: Orographic effects on airflow and mesoscale weather systems over Taiwan. *Terr. Atmos. Oceanic Sci.*, **4**, 381–420, doi:10.3319/TAO.1993.4.4.381(A).

Lin, Y. L., R. D. Farley, and H. D. Orville, 1983: Bulk parameterization of the snow field in a cloud model. *J. Climate Appl. Meteor.*, **22**, 1065–1092, doi:10.1175/1520-0450(1983)022<1065:BPOTSF>2.0.CO;2.

Maddox, R. A., 1976: An evaluation of tornado proximity wind and stability data. *Mon. Wea. Rev.*, **104**, 133–142, doi:10.1175/1520-0493(1976)104<0133:AEOTPW>2.0.CO;2.

——, 1983: Large-scale meteorological conditions associated with midlatitude, mesoscale convective complexes. *Mon. Wea. Rev.*, **111**, 1475–1493, doi:10.1175/1520-0493(1983)111<1475:LSMCAW>2.0.CO;2.

Markowski, P. M., 2002: Hook echoes and rear-flank downdrafts: A review. *Mon. Wea. Rev.*, **130**, 852–876, doi:10.1175/1520-0493(2002)130<0852:HEARFD>2.0.CO;2.

——, J. M. Straka, E. N. Rasmussen, and D. O. Blanchard, 1998: Variability of storm-relative helicity during VORTEX. *Mon. Wea. Rev.*, **126**, 2959–2971, doi:10.1175/1520-0493(1998)126<2959:VOSRHD>2.0.CO;2.

McCaul, E. W., Jr., D. E. Buechler, S. Hodanish, and S. J. Goodman, 2002: The Almena, Kansas, tornadic storm of 3 June 1999: A long-lived supercell with very little cloud-to-ground lightning. *Mon. Wea. Rev.*, **130**, 407–415, doi:10.1175/1520-0493(2002)130<0407:TAKTSO>2.0.CO;2.

McNider, R. T., and R. A. Pielke, 1981: Diurnal boundary-layer development over sloping terrain. *J. Atmos. Sci.*, **38**, 2198–2212, doi:10.1175/1520-0469(1981)038<2198:DBLDOS>2.0.CO;2.

Mead, C., and R. Thompson, 2011: Environmental characteristics associated with nocturnal significant-tornado events in the central and southern Great Plains. *Electron. J. Severe Storms Meteor.*, **6** (6). [Available online at http://www.ejssm.org/ojs/index.php/ejssm/article/view/84/66.]

Mlawer, E. J., S. J. Taubman, P. D. Brown, M. J. Iacono, and S. A. Clough, 1997: Radiative transfer for inhomogeneous atmospheres: RRTM, a validated correlated-*k* model for the longwave. *J. Geophys. Res.*, **102**, 16 663–16 682, doi:10.1029/97JD00237.

Moller, A. R., C. A. Doswell III, M. P. Foster, and G. R. Woodall, 1994: The operational recognition of supercell thunderstorm

environments and storm structures. *Wea. Forecasting*, **9**, 327–347, doi:10.1175/1520-0434(1994)009<0327:TOROST>2.0.CO;2.

Parish, T. R., and L. D. Oolman, 2010: On the role of sloping terrain in the forcing of the Great Plains low-level jet. *J. Atmos. Sci.*, **67**, 2690–2699, doi:10.1175/2010JAS3368.1.

Potvin, C. K., K. L. Elmore, and S. J. Weiss, 2010: Assessing the impacts of proximity sounding criteria on the climatology of significant tornado environments. *Wea. Forecasting*, **25**, 921–930, doi:10.1175/2010WAF2222368.1.

Przybylinski, R. W., J. T. Snow, E. M. Agee, and J. T. Curran, 1993: The use of volumetric radar data to identify supercells: A case study of June 2, 1990. *The Tornado: Its Structure, Dynamics, Prediction and Hazards*, *Geophys. Monogr.*, Vol. 79, Amer. Geophys. Union, 241–250.

Rasmussen, E. N., 2003: Refined supercell and tornado forecast parameters. *Wea. Forecasting*, **18**, 530–535, doi:10.1175/1520-0434(2003)18<530:RSATFP>2.0.CO;2.

——, and D. O. Blanchard, 1998: A baseline climatology of sounding-derived supercell and tornado forecast parameters. *Wea. Forecasting*, **13**, 1148–1164, doi:10.1175/1520-0434(1998)013<1148:ABCOSD>2.0.CO;2.

Shapiro, A., and E. Fedorovich, 2009: Nocturnal low-level jet over a shallow slope. *Acta Geophys.*, **57**, 950–980, doi:10.2478/s11600-009-0026-5.

——, ——, and S. Rahimi, 2016: A unified theory for the Great Plains nocturnal low-level jet. *J. Atmos. Sci.*, **73**, 3037–3057, doi:10.1175/JAS-D-15-0307.1.

Skaggs, R. H., 1969: Analysis and regionalization of the diurnal distribution of tornadoes in the United States. *Mon. Wea. Rev.*, **97**, 103–115, doi:10.1175/1520-0493(1969)097<0103:AAROTD>2.3.CO;2.

Skamarock, W. C., and Coauthors, 2008: A description of the Advanced Research WRF version 3. NCAR Tech. Note NCAR/TN-475+STR, 113 pp., doi:10.5065/D68S4MVH.

Smith, B. T., R. L. Thompson, A. R. Dean, and P. T. Marsh, 2015: Diagnosing the conditional probability of tornado damage rating using environmental and radar attributes. *Wea. Forecasting*, **30**, 914–932, doi:10.1175/WAF-D-14-00122.1.

Smith, R. B., 1979: The influence of mountains on the atmosphere. *Advances in Geophysics*, Vol. 21, Academic Press, 87–230, doi:10.1016/S0065-2687(08)60262-9.

Steiger, S. M., R. E. Orville, and L. D. Carey, 2007: Total lightning signatures of thunderstorm intensity over north Texas. Part I: Supercells. *Mon. Wea. Rev.*, **135**, 3281–3302, doi:10.1175/MWR3472.1.

Thompson, R. L., R. Edwards, J. A. Hart, K. L. Elmore, and P. Markowski, 2003: Close proximity soundings within supercell environments obtained from the Rapid Update Cycle. *Wea. Forecasting*, **18**, 1243–1261, doi:10.1175/1520-0434(2003)018<1243:CPSWSE>2.0.CO;2.

Weckwerth, T. M., L. J. Bennett, L. J. Miller, J. Van Baelen, P. D. Girolamo, A. M. Blyth, and T. J. Hertneky, 2014: An observational and modeling study of the processes leading to deep, moist convection in complex terrain. *Mon. Wea. Rev.*, **142**, 2687–2708, doi:10.1175/MWR-D-13-00216.1.

Weiss, J., and J. Zeitler, 2008: Supercells of the Serranías del Burro. *24th Conf. on Severe Local Storms*, Savannah, GA, Amer. Meteor. Soc., 17A.4. [Available online at https://ams.confex.com/ams/24SLS/techprogram/paper_141558.htm.]

Whiteman, C. D., X. Bian, and S. Zhong, 1997: Low-level jet climatology from enhanced rawinsonde observations at a site in the southern Great Plains. *J. Appl. Meteor.*, **36**, 1363–1376, doi:10.1175/1520-0450(1997)036<1363:LLJCFE>2.0.CO;2.

Zhong, S., J. Fast, and X. Bian, 1996: A case study of the Great Plains low-level jet using wind profiler network data and a high-resolution mesoscale model. *Mon. Wea. Rev.*, **124**, 785–806, doi:10.1175/1520-0493(1996)124<0785:ACSOTG>2.0.CO;2.